DOKUZ EYLÜL UNIVERSITY

GRADUATE SCHOOL OF NATURAL AND APPLIED SCIENCES

NUMERICAL INVESTIGATION OF ENCAPSULATED ICE THERMAL ENERGY STORAGE SYSTEM

by

Mehmet UZUN

July, 2014

İZMİR

NUMERICAL INVESTIGATION OF ENCAPSULATED ICE THERMAL ENERGY STORAGE SYSTEM

A Thesis Submitted to the
Graduate School of Natural and Applied Sciences of Dokuz Eylül University
In Partial Fulfillment of the Requirements for the Degree of Master of Science
in Mechanical Engineering, Thermodynamics Program
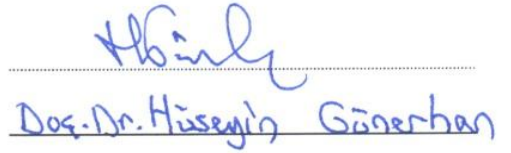
by
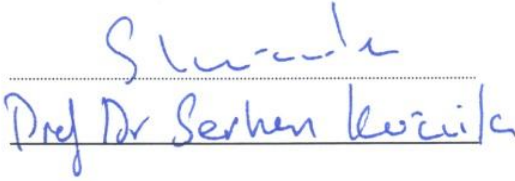**Mehmet UZUN**

July, 2014
İZMİR

ACKNOWLEDGMENTS

I would like to express my sincere gratitude to my advisor Assoc. Prof. Dr. Aytunç EREK, for the continuous support of my master study and research, for his patience, motivation, enthusiasm, and immense knowledge.

I also thank to Dr. M. Akif EZAN for significant contribution to the achievements of this work.

I also express my gratitude to my friends helping and supporting of my work and for their encouragement to me.

Finally, I thank to my family for supporting me throughout all my studies and my life.

Mehmet UZUN

NUMERICAL INVESTIGATION OF ENCAPSULATED ICE THERMAL ENERGY STORAGE SYSTEM

ABSTRACT

In this study, two different numerical solution methods are applied for phase change problems in one-dimensional cartesian coordinates. Solidification processes are simulated by using enthalpy method and temperature transformation method and predicted results are compared with the analytical one. Temperature distributions and time-wise variations of interface position are represented according to the determined boundary conditions. With respect to the results, increasing the number of nodes leads to increase the accuracy of the solution of the numerical methods. Highest discrepancies between the numerical and analytical results are observed near the interface position. In terms of accuracy and solution time, comparative results indicate that temperature transformation method gives better approximation.

The purpose of the second work is to evaluate effective thermal conductivity equations for inward melting problems inside spherical capsule in terms of the temperature difference and the spacing between the interface and the shell. Sets of numerical analyses have been carried out by commercial CFD software ANSYS-FLUENT. In order to validate the method, proposed effective thermal conductivity equation has been implemented into numerical code used MATLAB software. The results of the phase change problem inside a spherical capsule are compared with the experimental findings. Comparative results reveal that implementation of the effective thermal conductivity yields reasonable results regarding to the experimental measurements.

Keywords: Phase change, enthalpy method, temperature transformation method, effective thermal conductivity, natural convection

KAPSÜLLENMİŞ BUZ ISIL ENERJİ DEPOLAMA SİSTEMİNİN SAYISAL İNCELENMESİ

ÖZ

Bu çalışmada kartezyen koordinatlardaki bir boyutlu faz değişim problemi için iki farklı sayısal çözüm yöntemi kullanılarak uygulanan yöntemlerin doğruluğu belirlenmiştir. Entalpi metodu ve sıcaklık dönüşüm metodu kullanılarak katılaşma sırasındaki faz değişim süreci analitik yöntem ile karşılaştırılmıştır. Belirlenen sınır koşullara göre, sıcaklığın düğüm sayısına ve katı-sıvı ara yüzey konumunun zamana göre değişimi gösterilmiştir. Elde edilen sonuçlara göre düğüm sayısındaki artış sayısal yöntemlerin doğruluğunu arttırmıştır. Karşılaştırmalı sonuçlara göre yüzdesel hatanın en fazla olduğu konum faz değişiminin gerçekleştiği alandır. Sayısal yöntemlerin karşılaştırılması ile doğruluk ve çözüm zamanı açısından sıcaklık dönüşüm metodu diğer yönteme göre daha doğru sonuç vermiştir.

İkinci çalışmanın ana amacı küre içerisinde içe doğru erime probleminin efektif ısı iletim katsayısını denklemlerini elde etmektir. Sıvı fazdaki FDM'nin doğal taşınım modellemesi yapmak yerine, doğal taşınım etkisini efektif ısı iletim katsayısı kullanılarak elde edilmiştir. Efektif ısı iletim katsayısı için elde edilen denklemler iç küre yüzeyi ile dış küre yüzeyi arasındaki sıcaklık farkı ve uzunluk farkı cinsinden elde edilmiştir. Sayısal analizler ticari CFD yazılımı olan ANSYS-FLUENT programı ile gerçekleştirilmiştir. Metodun doğruluğunu kontrol etmek için ısı iletim katsayısı denklemleri MATLAB programı kullanılarak yazılan küresel koordinatlardaki faz değişim problem kodu kullanılmıştır. Hesaplanan sonuçlar deneysel verilerle karşılaştırılmıştır. Karşılaştırılmalı sonuçlardan elde edildiği üzere efektif ısı iletim katsayısının uygun sonuçlar verdiği gözlemlenmiştir.

Anahtar kelimeler: Faz değişimi, entalpi yöntemi, sıcaklık dönüşüm yöntemi, efektif ısı iletim katsayısı, doğal taşınım

CONTENTS

LIST OF FIGURES

LIST OF TABLES

CHAPTER ONE
INTRODUCTION

1.1 General Introduction

Depending on the growing population and energy demand, the usage of fossil fuels is increased. Due to increasing the greenhouse emissions, utilization of different types of renewable energy sources such as solar, wind etc. have revealed. However the main problem of the application of renewable energy sources is their sustainability. Energy storage systems are gaining prominence as a solution for ensuring sustainability of renewable energy sources. Energy storage contributes significantly to fulfil society's needs as environmentally harmless energy usage and more efficient systems. Energy storage systems have great benefits as reduced energy cost, energy consumption, pollutant emissions. Energy can be stored in different ways which is classified in following forms: mechanical, thermal, chemical and electrical as shown in Figure 1.1.

```
Energy Storage Methods
        |
        |—— Mechanical Energy Storage
        |
        |—— Chemical Energy Storage
        |
        |—— Thermal Energy Storage
        |
        |—— Electrical Energy Storage
```
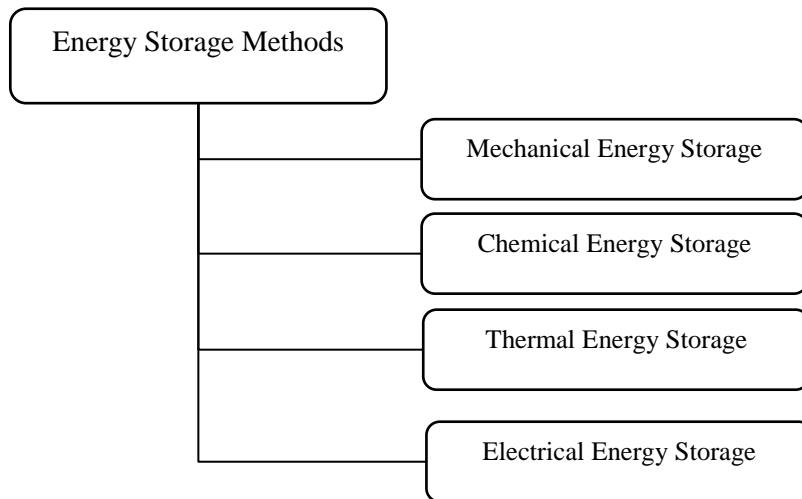
Figure 1.1 A classification of energy storage methods

Mechanical energy can be stored as kinetic energy, potential energy and strain energy in order of rotational or linear motion, elevated object and elastical materials.

Chemical energy storage is generally used in batteries, interaction between compounds cause emerging energy. Electrical energy is a force that movement of the electrons in an atomic structure. Electrical energy can be stored in a capacitor or in a magnetic field. Thermal energy is sum of the potential and kinetic energy of the atoms or molecules which constitutes a material. Thermal energy is stored by changing internal energy of the material.

Energy conservation and improving utilization of the systems have a great importance. Thermal energy storage (TES) has a significant role in many thermal systems. TES systems are aimed to reduce energy demand while energy usage intense at that time.

1.2 Thermal Energy Storage and Appliances

The first prominent usage of the thermal energy storage systems is solar power systems. Solar power has not permanence unlike fossil fuels. Solar power systems are combined with thermal energy storage to overcome the discontinuity. These systems are provides energy storage for later usage at low or high temperatures. For instance; combination of the TES systems with solar power, energy stored at the daytime and the energy that is stored is reused at night.

Simple thermal energy storage system demonstration is shown in Figure 1.2. Thermal energy storage systems (TES) consist of three main parts. These are charging, storing and discharging. In real situations charging and storing processes occur at the same time.
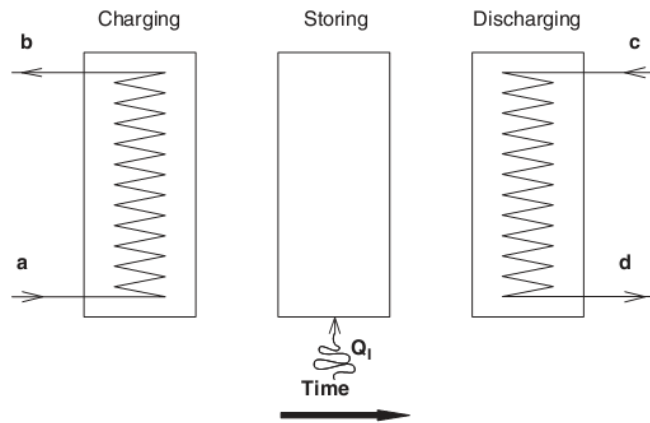
Figure 1.2 Simple thermal energy storage system

1.2.1 Sensible Thermal Energy Storage

Sensible thermal energy storage systems use temperature differences of the storage area (water, air, oil, bedrock, clay, sand, soil, etc.). Sensible heat in the TES systems related to initial and final temperature differences of the storage area.

Sensible TES materials are encountered storage operation while temperature changes without phase change. Total heat stored in a mass is defined as;

$$Q = mc_p\left(T_2 - T_1\right) = \rho V c_p\left(T_2 - T_1\right) \tag{1.1}$$

T_1 and T_2 are referred as initial and final temperature of the TES materials. Storage capacity of the sensible TES materials is dependent the amount of ρc_p.

1.2.2 Latent Thermal Energy Storage

Energy is stored in a material as latent heat thermal energy storage during the phase change processes. With this purpose, phase change materials (PCM) recover heat by absorbing heat or releasing heat in the ambient at the constant phase change temperature. Stored energy during the melting or solidification process cannot be evaluated because phase change process occurs at a single temperature value.

3

Meanwhile provided heat is called as latent heat, the process of the storing latent heat is called as latent heat thermal energy storage. Storing heat in a mass is evaluated as;

$$\Delta Q = \Delta H = m \, \Delta h \qquad (1.2)$$

Δh defines latent heat in a unit mass. Latent heat thermal energy storage has some advantages according to sensible heat thermal energy storage. PCM have bigger storage capacity in unit mass or unit volume in comparison with sensible thermal energy storage materials. The storage tank volume that used for latent heat thermal energy storage systems is smaller than sensible heat thermal energy storage to storing the same amount of energy. During the energy storage, the appliance of heat storage and recovery at constant temperature value is suitable for phase change problem.

1.3 Literature Review

Voller & Prakash (1987) studied two-dimensional phase change problems in rectangular region. They developed numerical solution of the phase change problem using enthalpy method (EM). In numerical solution method three different phases take in account. These are solid, liquid and mushy region. Mushy region is where phase change process occurs in the solidification problem. Dimensionless parameters considered and specific heat, density, thermal conductivity and viscosity taken as constant. That means these parameters do not change in different phase (solid, liquid and mushy). Researchers aimed the modelling the mushy region for phase change problems and they demonstrated the flow distributions and thermal isotherms for the phase change problems which is integrated mushy zone.

Voller & Swaminathan (1991) investigated source-based method which is used for enthalpy calculation for solidification phase change problems. The feature of the source-based method is linearization of the source term. In the source-based method latent heat term calculated every iteration according to liquid fraction. Also in this paper source-based method compared with apparent heat capacity method. As a

result of this comparison source-based method gives better result with respect to accuracy, time of solution and number of iterations.

Bilir & Ilken (2005) present numerical solution of the solidification process of the phase change problem. As a numerical solution enthalpy method and control volume approach is used in the problem. Researchers determined dimensionless total solidification time of the phase change materials inside spherical or cylindrical container. They also found correlation of the total solidification time in terms of Stefan number and Bi number.

Cao & Faghri (1990) investigate numerical analysis of phase chance problems including natural convection. Temperature transformation method which is developed by Cao and Faghri is used as a numerical method. The most significant feature of the temperature transformation method (TTM) is that energy equation is described as a function of temperature. TTM is applicable for phase change occurs in a single temperature point or over a temperature range. The accuracy of the method is assured using exact solution of the one-dimensional melting problem.

Cao & Faghri (1991) modelled two-dimensional PCM included concentric cylindrical containers. In this study aimed to optimization such a system with annular and counter-current flow. Temperature transformation method is integrated into the energy equation to solving phase change process. Using temperature transformation method solid, liquid and mushy phase is considered. Latent heat term is included in mushy phase and liquid phase. Mushy phase is defined as transition region and occurred in a small temperature range. Numerical analysis of the governing equation is solved by using control volume approach. Residual values of the continuity, momentum and energy are ensured less than 10^{-5}. As a result of temperature distribution for different time periods, counter flow and annular flow of the mathematical model is compared according to interface position. Counter-current flow increases energy storage capacity with respect to annular flow.

Bishop, Mack & Scanlan (1966) investigate natural convection of the two concentric spheres experimentally which has air inside. They determined different annulus length while changing inner sphere diameter. Different spacing ratios are determined to visualize the flow pattern and temperature pattern. With the experimental visualizations three different type of flow pattern are observed. After observation the flow pattern different air flow shapes occur. These are; kidney-shaped eddy, falling vortices and crescent-eddy flow. The aim of this study, evaluate Nusselt number correlations depending of the spacing ratio and Grashof number. Obtained Nusselt number correlations are compared with the experimental data and results are shows proximity between -14% to +25%.

Ismail, Hernandez, & Silva (2003) modelled phase change process in spherical capsule and numerical investigation of the solidification process is achieved. Finite difference approach and moving grid scheme are used to solve numerical method. Also they used the different capsule diameter and capsule material to determine effect of the capsule size on total solidification time. But in their study, instead of modelling natural convection, they used constant effective thermal conductivity. Using effective thermal conductivity, numerical solution shows consistency with experimental data.

Assis, Katsman, Ziskind, & Letan (2007) are studied spherical capsule melting time which has paraffin inside experimentally and numerically. Spherical capsule have paraffin as a PCM also top of the capsule exist air to overcome volume change. Spherical capsule are designed as unconstrained and for comparison numerical solution are managed using commercial CFD software ANSYS-FLUENT. Suitable time step for numerical analysis are taken 0.002 s. Melt fraction of the PCM are compared numerically and experimentally.

1.4 Objectives, Motivation and Methodology

The main objective of this study is to compare the numerical methods in terms of suitability and accuracy for phase change problems. Enthalpy method (EM) and

temperature transformation method (TTM) are determined to solve phase change problems. Enthalpy method is developed by Voller & Prakash (1987) to solve phase change problems for three phases solid, mushy and liquid. Temperature transformation method is improved by Cao & Faghri (1990) defining enthalpy function in terms of specific heat and source term. Validation of the methods is explained clearly in the Chapter 2. Comparison of the methods is identified using analytical solution during the phase change process. Comparisons are achieved according to temperature distributions and solid-liquid interface location. Parametric study of the TTM is applied Bi number and Stefan number variations.

The other objective of the study is evaluating the effective thermal conductivity of water inside the sphere. There are countless studies which deal with the numerical and experimental investigation of natural convection driven phase change. One of them is Bishop (1966) is considered concentric sphere different spacing ratio to evaluate the Nusselt correlations with respect to spacing ratio and Grashof number. Our aim is simplifying natural convection driven phase change problems. Instead of modelling natural convection for the liquid phase of the PCM, effective thermal conductivity is defined to consider the influence of convection. Different annulus ratios are considered for steady state natural convection in concentric spheres.

CHAPTER TWO
NUMERICAL METHODS OF ONE-DIMENSIONAL
PHASE CHANGE PROBLEMS

2.1 Problem Definition of One-Dimensional Phase Change Problems

In this research, our first aim is to exhibit the numerical methods of the phase change problems as mentioned before. While discussing the numerical methods of phase change problems, the advantage and disadvantage of the numerical methods are examined. The problem is compared as the accuracy of the solution of temperature and interface position and solution time.

Investigating the numerical methods, we deal with one dimensional solidification problem. One dimensional phase change problem in cartesian coordinates is shown in Figure 2.1.
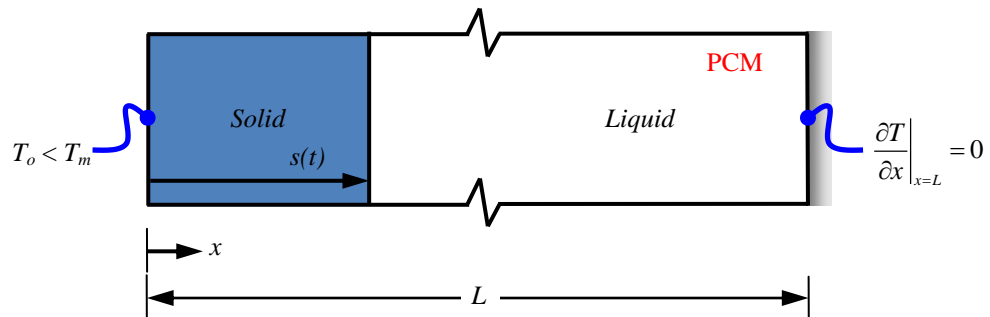
Figure 2.1 One-dimensional cartesian coordinate phase change model

The problem consist of the following assumptions,
1. One dimensional heat conduction is considered,
2. Constant thermo-physical properties of the PCM in the same phases,
3. Natural convection is negligible,

In Figure 2.1 one dimensional phase change model in cartesian coordinate is defined and phase change material is existed in a system in length of *L*. At the beginning, phase change material (PCM) is in liquid form and the temperature of the

PCM is higher than melting temperature ($T_i > T_m$) in the system. One surface of the domain ($x = L$) is isolated and the other surface temperature is suddenly reduced to T_o temperature which is lower than melting temperature ($T_o < T_m$). At that time, the solidification process (phase change process) starts in the cold surface. While time progressing, interface location, $s(t)$, of the phase change material is moving x–direction. When interface location reaches $x = L$ the solidification process of the phase change material is completed.

Table 2.1 Boundary condition of the one-dimensional cartesian coordinate phase change problem

$T(x,t) = T_o(x,t)$	$x = 0$	$t > 0$
$\dfrac{\partial T}{\partial x} = 0$	$x = L$	$t > 0$

Boundary condition of the one dimensional cartesian coordinates phase change problem is shown in Table 2.1. The first row demonstrates the temperature of the surface is equal to initial temperature. In the second row, with the progressing time temperature of the surface wall is equal to T_o which is lower than initial temperature, T_i. The last row shows that the surface of $x = L$ is isolated and the meaning of that there is no heat transfer on this surface with the progressing time.

The other phase change model is solidification problem of one dimensional spherical coordinates as shown in Figure 2.2.
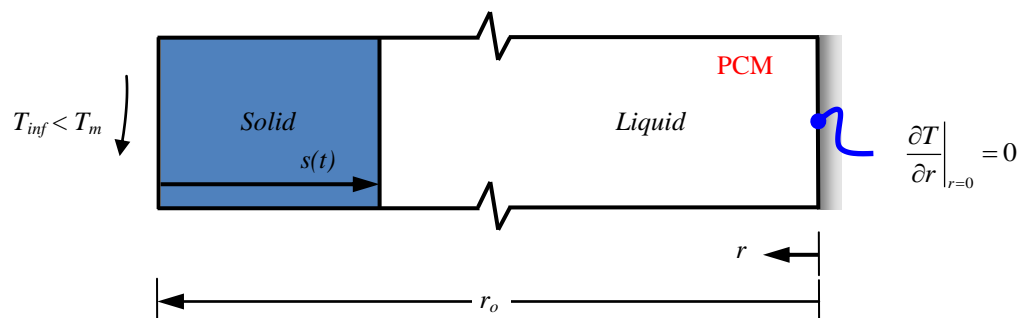
Figure 2.2 One-dimensional spherical coordinate phase change model

9

The problem consist of the following assumptions,

1. One dimensional heat conduction is considered,
2. Constant thermo-physical properties of the PCM in the same phases,
3. Natural convection is negligible,

In Figure 2.2 one dimensional phase change model in spherical coordinate is defined and phase change material is existed in a system in length of r_o. At the beginning phase change material (PCM) is in liquid form and the temperature of the PCM is higher than melting temperature ($T_i > T_m$) in the system. One surface of the system when $r=0$ is isolated and the sphere is suddenly submerged into ambience which has heat transfer fluid of T_{inf}. The temperature of the heat transfer fluid is lower than melting temperature ($T_{inf} < T_m$). At that time, the solidification process (phase change process) starts in the cold surface. While time progressing, interface location, $s(t)$, of the phase change material is moving r–direction. When interface location reaches $r=0$ the solidification process of the phase change material is completed.

Table 2.2 Boundary condition of the one-dimensional spherical coordinate phase change problem

$-k\dfrac{\partial T}{\partial r}\Big|_{r=r_o} = h\left(T - T_{\text{inf}}\right)$	$r= r_o$	$t>0$
$\dfrac{\partial T}{\partial r} = 0$	$r=0$	$t>0$

Boundary condition of the one dimensional phase change problem in spherical coordinates is shown in Table 2.2. In the first row, it demonstrates the temperature of the surface is equal to initial temperature with respect to radius and time. In the second row, with the progressing time convection heat transfer is included at $r= r_o$. The temperature of the surface wall changes according to equation which is shown in second row Table 2.2. Convection heat transfer is equal to conduction heat transfer at the surface. Convection heat transfer coefficient and ambient temperature, T_{inf}, depended on the heat transfer withdrawn from surface. The last row with the

progressing time shows that the surface of $r= 0$ is isolated and the meaning of that there is no heat transfer on this surface.

2.2 Analytical and Numerical Methods of Phase Change Problems

'Phase change problem' or 'moving boundary problem' is a time dependent heat transfer problem including solidification or melting phenomena. Phase change problems have non-linear characteristics therefore analytic or semi-analytical solutions are obtained for only a limited number of simplified problems (Lunardini, 1981 & Ozişik, 1993). Besides, some researches try to figure out two dimensional phase change problems using analytical solutions (Poots, 1962, Rathjen & Jiji, 1970). But these studies are accomplished for special or simple geometries. In general analytical solutions cannot be applied for two or three dimensional phase change problem geometries. Therefore solution of many phase change problems can be achieved by use of numerical methods. Most common use of numerical methods for phase change problems are temperature transformation method (TTM) and enthalpy method (EM). Enthalpy method comes into prominence as general approach to solving phase change problems.

2.2.1 Analytical Method of Phase Change Problems (Two-Region Problem)

Carslaw & Jaeger (1959) improve exact solution of the one dimensional phase change problems in semi-infinite region. In the problem two region phase change which consist of solid and liquid phase take in account. While calculating the two-region phase change problem three state taken into consideration. These are conduction in solid phase, conduction in liquid phase and heat transfer at the interface location where the phase change occur.

At the beginning phase change material is in liquid phase and at the uniform temperature of T_i. The initial temperature of the phase change material is higher than T_m melting temperature. Problem at the time of $t=0$ surface temperature where is at $x=0$ is decreased T_o temperature which is lower than melting temperature. While the

time is progressing, solidification start with the boundary surface *x=0*. The phase change solid-liquid interface location *x=s(t)* is moving positive x direction.
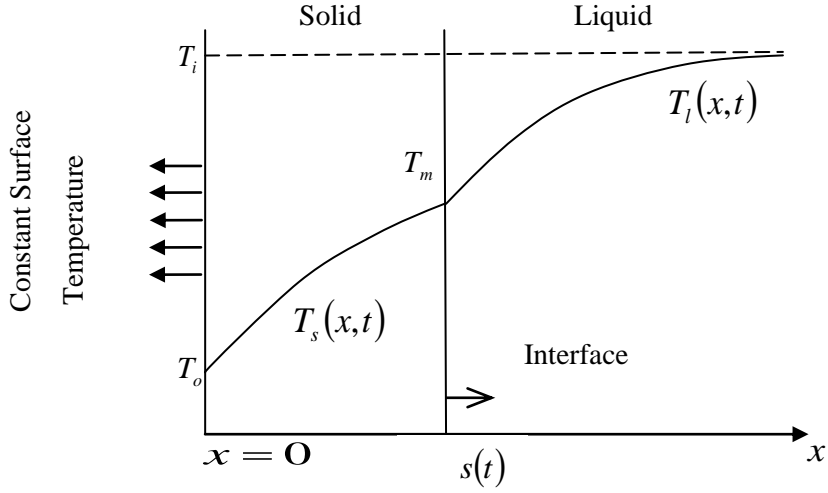
Figure 2.3 Analytical solution two-region problem definition

In Figure 2.3 shows temperature distribution of the one dimensional solidification problem. Also interface movement described along x-direction. Temperature of $T_s(x,t)$ and $T_l(x,t)$ for solid and liquid phase obtained using heat conduction equation shown in Equation 2.1 and 2.2.

$$\frac{\partial^2 T_s(x,t)}{\partial x^2} = \frac{1}{\alpha_s} \frac{\partial T_s(x,t)}{\partial t} \qquad\qquad 0 < x < s(t) \qquad\qquad (2.1)$$

$$\frac{\partial^2 T_l(x,t)}{\partial x^2} = \frac{1}{\alpha_l} \frac{\partial T_l(x,t)}{\partial t} \qquad\qquad s(t) < x < \infty \qquad\qquad (2.2)$$

Phase change material assumed constant thermal properties in solid and liquid phase separately. Phase change interface location is defined as *s(t)*. Besides '*s*' and '*l*' terms define solid and liquid phase respectively. Problem has three unknown variable: solid phase temperature $T_s(x,t)$, liquid phase temperature $T_l(x,t)$ and solid-liquid interface location *s(t)*. Determining the phase change interface location, energy conservation equation is used to find *x=s(t)* location.

12

$$
\begin{bmatrix}
\textit{Negative } x - \textit{direction} \\
\textit{diffusion heat flux in solid phase}
\end{bmatrix}
-
\begin{bmatrix}
\textit{Negative } x - \textit{direction} \\
\textit{diffusion heat flux in fluid phase}
\end{bmatrix}
$$
$$
=
\begin{bmatrix}
\textit{Released heat in unit area} \\
\textit{during solidification}
\end{bmatrix}
$$

or

$$
k_s \frac{\partial T_s(x,t)}{\partial x} - k_l \frac{\partial T_l(x,t)}{\partial x} = \rho L \frac{ds(t)}{dt}
\qquad (2.3)
$$

L is defined as latent heat or heat of fusion. Density change for solid and liquid phase is neglected and interface temperature is written as additional condition as follows;

$$
T_s(x,t) = T_l(x,t) = T_m \qquad\qquad at \qquad x = s(t) \qquad (2.4)
$$

Mathematical formulation of one-dimensional phase change problem including boundary condition and initial condition is presented in Equation 2.5 - 2.11.

Solid phase condition;

$$
\frac{\partial^2 T_s(x,t)}{\partial x^2} = \frac{1}{\alpha_s} \frac{\partial T_s(x,t)}{\partial t} \qquad\qquad 0 < x < s(t) \qquad\qquad t > 0 \qquad (2.5)
$$

$$
T_s(x,t) = T_0 \qquad\qquad\qquad x = 0 \qquad\qquad t > 0 \qquad (2.6)
$$

Liquid phase condition;

$$
\frac{\partial^2 T_l(x,t)}{\partial x^2} = \frac{1}{\alpha_l} \frac{\partial T_l(x,t)}{\partial t} \qquad\qquad s(t) < x < \infty \qquad\qquad t > 0 \qquad (2.7)
$$

$$
T_l(x,t) = T_i \qquad\qquad\qquad x \rightarrow \infty \qquad\qquad t > 0 \qquad (2.8)
$$

13

$$T_l(x,t) = T_i \qquad\qquad x > 0 \qquad\qquad t = 0 \qquad\qquad (2.9)$$

Solid-liquid interface condition;

$$T_s(x,t) = T_l(x,t) = T_m \qquad\qquad x = s(t) \qquad t > 0 \qquad (2.10)$$

$$k_s \frac{\partial T_s(x,t)}{\partial x} - k_l \frac{\partial T_l(x,t)}{\partial x} = \rho \Delta h \frac{ds(t)}{dt} \qquad\qquad x = s(t) \qquad t > 0 \qquad (2.11)$$

Temperatures of solid and liquid phase are calculated using Equation 2.12 and 2.13.

$$T_s(x,t) = T_0 + A\,erf\left[x / 2(\alpha_s t)^{1/2} \right] \qquad\qquad (2.12)$$

$$T_l(x,t) = T_i + B\,erfc\left[x / 2(\alpha_l t)^{1/2} \right] \qquad\qquad (2.13)$$

T_s and T_l temperatures are equals at the solid-liquid interface location. Therefore the equation of phase change temperature is obtained with respect to initial and surface temperature in Equation 2.14.

$$T_0 + A\,erf(\lambda) = T_i + B\,erfc\left[\lambda \left(\frac{\alpha_s}{\alpha_l} \right)^{1/2} \right] = T_m \qquad\qquad (2.14)$$

where

$$s(t) = 2\lambda(\alpha_s t)^{1/2} \qquad\qquad (2.15)$$

A and B coefficients can be calculated using Equation 2.16 and 2.17.

$$A = \frac{T_m - T_0}{erf(\lambda)} \tag{2.16}$$

$$B = \frac{T_m - T_i}{erfc\left[\lambda\left(\dfrac{\alpha_s}{\alpha_l}\right)^{1/2}\right]} \tag{2.17}$$

When *A* and *B* coefficients put into the equation 2.12 and 2.13, temperature equations of the solid and liquid phase are found in Equation 2.18 and 2.19.

$$\frac{T_s(x,t) - T_0}{T_m - T_0} = \frac{erf\left[x/2(\alpha_s t)^{1/2}\right]}{erf(\lambda)} \tag{2.18}$$

$$\frac{T_l(x,t) - T_i}{T_m - T_i} = \frac{erfc\left[x/2(\alpha_l t)^{1/2}\right]}{erfc\left[\lambda(\alpha_s/\alpha_l)^{1/2}\right]} \tag{2.19}$$

λ parameters are calculated using transcendental equation shown in Equation 2.20. This transcendental equation is obtained using Equation 2.15, 2.18 and 2.19.

$$\frac{e^{-\lambda^2}}{erf(\lambda)} + \frac{k_l}{k_s}\left(\frac{\alpha_s}{\alpha_l}\right)^{1/2} \frac{T_m - T_i}{T_m - T_0} \frac{e^{-\lambda^2(\alpha_s/\alpha_l)}}{erfc\left[\lambda(\alpha_s/\alpha_l)^{1/2}\right]} = \frac{\lambda \Delta h \sqrt{\pi}}{C_{ps}(T_m - T_0)} \tag{2.20}$$

2.2.2 Numerical Methods of Phase Change Problems

In this section, we figure out the numerical methods of phase change problems described chapter 2.1. In the engineering application, there are different ways to discretizate the differential equations. These are; finite difference, finite element and finite volume methodology. In this study, finite volume methodology are used to discrete the differential equations because FVM is generally used with phase change problems to integrating governing equations.

2.2.2.1 Finite Volume Methodology

Finite volume methodology is a discretazation method of the solution of differential equations. The solution of the problem that expressed differential equations is discreted particular number of finite volume. Finite volume or control volume constitutes the background of the solution method for commercial computational fluid dynamic software. Conservation equations are applied every number of discretized control volumes (Versteeg H.K., Malalasekara W.,1995).

One dimensional heat conduction problem in cartesian and spherical coordinate domain is described in the following problem.

General form of one dimensional energy equation;

$$\frac{\partial H^*}{\partial t} = \frac{1}{r^n} \frac{\partial}{\partial r}\left(kr^n \frac{\partial T}{\partial r}\right) \tag{2.21}$$

Next step, discretization equations for cartesian, cylindrical and spherical coordinates are demonstrated in the following section. Equation 2.21 shows energy equation that for $n=0$ cartesian coordinate, $n=1$ cylindrical coordinate and $n=2$ spherical coordinate. Entalpy is expressed as in Equation 2.22.

$$H^* = cT + s \tag{2.22}$$

where, c is specific heat, T temperature and s is a source term. When we combine enthalpy formulation with Equation 2.21 defined as,

$$\frac{\partial(cT)}{\partial t} + \frac{\partial(s)}{\partial t} = \frac{1}{r^n} \frac{\partial}{\partial r}\left(kr^n \frac{\partial T}{\partial r}\right) \tag{2.23}$$

where, k is thermal conductivity. The selected solution domain is shown in Figure 2.4.
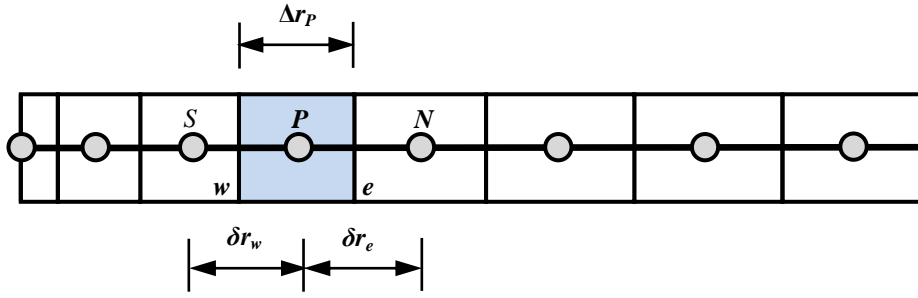
Figure 2.4 Control volume and grid notation

Figure 2.4 demonstrate incremental control volume and grid notation. After dividing control volume, central point of the control volume notate as P. The neighbour control volume west and east called as W and E. Small letters w and e points indicate surface of the control volumes (Versteeg H.K., Malalasekara W.,1995).

Equation 2.23 integrated along the control volume which central grid point P,

$$\int\limits_{w}^{e}\int\limits_{t}^{t+\Delta t} \frac{\partial}{\partial t}(cT)\,dt\,d\forall = \int\limits_{t}^{t+\Delta t}\int\limits_{w}^{e} \frac{1}{r^n}\frac{\partial}{\partial r}\left(kr^n\frac{\partial T}{\partial r}\right)d\forall\,dt - \int\limits_{w}^{e}\int\limits_{t}^{t+\Delta t}\frac{\partial s}{\partial t}\,dt\,d\forall \qquad (2.24)$$

where, differential volume for cartesian, cylindrical and spherical coordinates as follows,

$$d\forall = dr \qquad\qquad \text{cartesian coordinate} \qquad (2.25)$$
$$d\forall = 2\pi r\,dr \qquad\qquad \text{cylindrical coordinate} \qquad (2.26)$$
$$d\forall = 4\pi r^2\,dr \qquad\qquad \text{spherical coordinate} \qquad (2.27)$$

Equation 2.24 rearranged according to differential volume shown in Equation 2.25, 2.26 and 2.27.

$$\left(cT_p - c^oT_P^o\right)\left(\frac{r_e^{n+1} - r_w^{n+1}}{n+1}\right) + \left(s - s^o\right)\left(\frac{r_e^{n+1} - r_w^{n+1}}{n+1}\right) = \left[\left(kr^n\frac{\partial T}{\partial t}\right)_e - \left(kr^n\frac{\partial T}{\partial t}\right)_w\right]dt \qquad (2.28)$$

$$\left(\frac{cT_p - c^oT_P^o}{\Delta t}\right)\left(\frac{r_e^{n+1} - r_w^{n+1}}{n+1}\right) + \left(\frac{s - s^o}{\Delta t}\right)\left(\frac{r_e^{n+1} - r_w^{n+1}}{n+1}\right) = \left[k_e r_e^{\;n}\left(\frac{T_E - T_P}{\Delta r_e}\right) - k_w r_w^{\;n}\left(\frac{T_P - T_W}{\Delta r_w}\right)\right] \quad (2.29)$$

Equation 2.28 and 2.29 shows the rearranged discretized formulations. *P*, *E* and *W* notations shows center, east and west point of the control volume respectively. Superscript is shown as '*o*' describes the variables at the previous time step.

where,

$$\Delta r_{ew} = \frac{r_e^{n+1} - r_w^{n+1}}{n+1} \tag{2.30}$$

Then, the last rearranged general form of the equation described Equation 2.31.

$$T_P\left(\frac{k_e r_e^{\;n}}{\Delta r_e} + \frac{k_w r_w^{\;n}}{\Delta r_w} + \frac{c\Delta r_{ew}}{\Delta t}\right) = \frac{k_e r_e^{\;n}}{\Delta r_e}T_E + \frac{k_w r_w^{\;n}}{\Delta r_w}T_W - \left(\frac{s - s^o}{\Delta t}\right)\Delta r_{ew} + \frac{c^oT_P^o}{\Delta t} \tag{2.31}$$

Equation 2.31 can be written as a matrix form and matrix coefficients a_P, a_E, a_W are defined in Equation 2.32.

$$a_P T_P = a_E T_E + a_W T_W + b \tag{2.32}$$

Equation 2.33 to 2.37 presents formulation of the coefficient matrix. S_u and b term is calculated from Equation 2.31. Equation 2.24, 2.31 and 2.32 present the discretization of equation. (Patankar 1980)

$$a_E = \left[\frac{k_e r_e^{\;n}}{\Delta r_e}\right] \tag{2.33}$$

$$a_W = \left[\frac{k_w r_w^{\;n}}{\Delta r_w}\right] \tag{2.34}$$

$$S_u = \left[-c^o \frac{\Delta r_{ew}}{\Delta t}\right] \tag{2.35}$$

$$a_p = \left[a_E + a_W - S_u\right] \tag{2.36}$$

$$b = \left[c\frac{\Delta r_{ew}}{\Delta t} \right] T_P^o + \left(\frac{s^o - s}{\Delta t} \right) \Delta r_{ew} \tag{2.37}$$

When the solidification front reaches 'e' shown in Figure 2.5, thermal properties of the control volumes pointed as P and E is different each other. In this case different thermal conductivity should be defined at the solid-liquid interface location. Therefore calculation of the thermal conductivity of the coefficient matrix k_e and k_w is used thermal conductivity of the neighbour control volumes. Most common thermal conductivity calculation for interface location is harmonic mean developed by Patankar (1980).
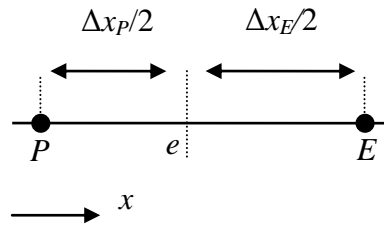
Figure 2.5 Interface position (Cartesian coordinate)

Figure 2.5 shows that notation of interface position for cartesian coordinate. The notation of e represents control volume surface and calculation of the thermal conductivity at that point is indicated Equation 2.38.

$$k_e = \frac{k_P k_E}{k_P \, \Delta x_E / \Delta x_P + k_E \left(1 - \Delta x_E / \Delta x_P \right)} \tag{2.38}$$

19
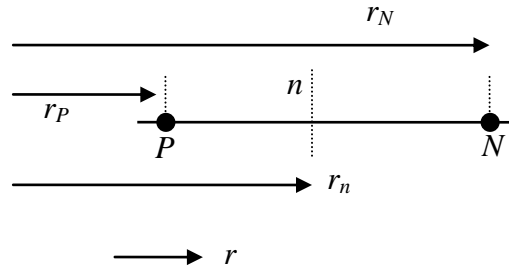
Figure 2.6 Interface position (Spherical coordinate)

Figure 2.6 shows that notation of interface position for spherical coordinate. The notation of n represents control volume surface and calculation of the thermal conductivity at that point is indicated Equation 2.39.

$$k_n = \frac{\left(\dfrac{1}{r_N} - \dfrac{1}{r_P} \right)}{\dfrac{1}{k_N} \left(\dfrac{1}{r_N} - \dfrac{1}{r_n} \right) + \dfrac{1}{k_P} \left(\dfrac{1}{r_n} - \dfrac{1}{r_P} \right)} \qquad (2.39)$$

2.2.2.2 Dimensionless Form of Equations

Governing equations rearranged according to dimensionless variables because non-dimensional equations are easy to solve on the contrary of dimensional form. Table 2.3 shows that dimensionless variables that used in equations and functions.

Non-dimensional form of energy equation shown in Equation 2.40

$$\frac{\partial H}{\partial \tau} = \frac{1}{R^n} \frac{\partial}{\partial R} \left(KR^n \frac{\partial \theta}{\partial R} \right) \qquad (2.40)$$

Table 2.3 Dimensionless variables

	Dimensional form	Dimensionless form
Time	t	$\tau = \dfrac{\alpha_l t}{r^2}$
Radius	r	$R = \dfrac{r}{r_o}$
Temperature	T	$\theta = \dfrac{T - T_m}{T_{in} - T_m}$
Phase change temperature range	δT	$\delta\theta = \dfrac{\delta T}{T_{in} - T_m}$
Enthalpy	H^*	$H = \dfrac{H^*}{c_l\left(T_{in} - T_m\right)}$
Thermal conductivity	k	$K = \dfrac{k}{k_l}$
Heat capacity	ρc	$C = \dfrac{\rho c}{\left(\rho c\right)_l}$
Source term	s	$S = \dfrac{\rho s}{\left(\rho c\right)_l\left(T_{in} - T_m\right)}$
Stefan number	-	$Ste = \dfrac{c_l\left(T_{in} - T_m\right)}{\Delta H}$

Equation 2.41 shows that the dimensionless form of Equation 2.24 according to Table 2.3.

$$\int_w^e \int_\tau^{\tau+\Delta\tau} \frac{\partial}{\partial\tau}\left(C\theta\right) d\tau d\forall = \int_\tau^{\tau+\Delta\tau} \int_w^e \frac{1}{R^n}\frac{\partial}{\partial R}\left(kR^n\frac{\partial\theta}{\partial R}\right) d\forall d\tau - \int_w^e \int_\tau^{\tau+\Delta\tau} \frac{\partial S}{\partial\tau} d\tau d\forall \qquad (2.41)$$

Dimensionless matrix form of discritized equation,

$$a_P\theta_P = a_E\theta_E + a_W\theta_W + b \qquad (2.42)$$

Equation 2.43 to 2.47 indicates the non-dimensional form of coefficients of the Equation 2.42.

21

$$a_E = \left[\frac{K_e R_e{}^n}{\Delta R_e} \right]$$ (2.43)

$$a_W = \left[\frac{K_w R_w{}^n}{\Delta R_w} \right]$$ (2.44)

$$S_u = \left[-C^o \frac{\Delta R_{ew}}{\Delta \tau} \right]$$ (2.45)

$$a_p = \left[a_E + a_W - S_u \right]$$ (2.46)

$$b = \left[C \frac{\Delta R_{ew}}{\Delta \tau} \right] \theta_P^o + \left(\frac{S^o - S}{\Delta \tau} \right) \Delta R_{ew}$$ (2.47)

2.2.2.3 Enthalpy Method

In this methodology, governing equation should be written for solid, liquid and mushy phases. Total enthalpy 'H' is the summation of sensible heat and latent heat shown in Equation 2.48.

$$H = h + \Delta H$$ (2.48)

Voller and Prakash (1987) defined a function to calculate the latent heat effect for solid, mushy and liquid phases. This function is written in terms of temperature demonstrated at Equation 2.49.

$$\Delta H = f\left(\theta \right)$$ (2.49)

This $f(\theta)$ function take in consideration for solid, liquid and mushy phases and this function presented non-dimensional form in Equation 2.50. St is Stefan number which is proportional of sensible heat to latent heat.

$$f\left(\theta \right) = \begin{cases} 0 & \theta < -\delta\theta \\ 1/St(1-(\theta)) & -\delta\theta < \theta < \delta\theta \\ 1/St & \theta > \delta\theta \end{cases}$$ (2.50)
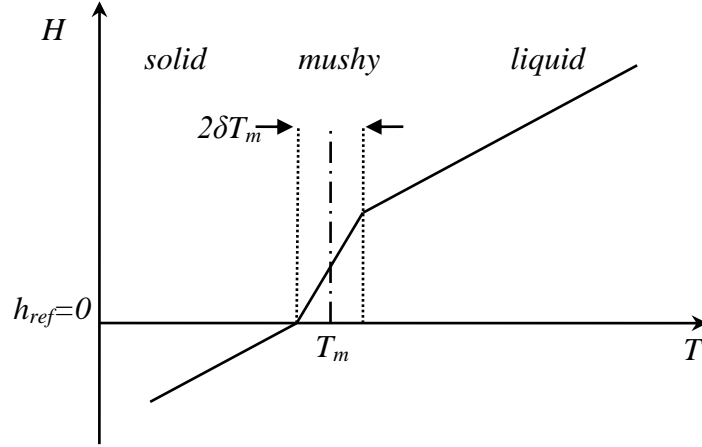
Figure 2.7 Enthalpy-temperature relations for phase change problem

$$H^* = h_{ref} + \int_{T_{ref}}^{T} \rho c_p dT + f\left(\rho \Delta H^*\right) \qquad (2.51)$$

h_{ref} is the reference enthalpy, f is the solidification rate and Equation 2.51 show the enthalpy change in unit volume. Figure 2.7 and Equation 2.51 examined together, it shows that in solid phase sensible heat take in account in calculation. In mushy region sensible heat and latent heat considered but latent heat is calculated according to solidification rate. In liquid phase, all of the PCM is melted therefore sensible and latent heat count in calculation.

Solid Phase, $(T < T_m - \delta T_m)$

$$H^*(T) = 0 + \int_{T_{ref}}^{T} \rho_s c_{ps} dT + 0 \qquad (2.52)$$

$$H^*(T) = \left(\rho c_p\right)_s \left[T - \left(T_m - \delta T_m\right)\right] \qquad (2.53)$$

Mushy Phase, $(T_m - \delta T_m < T < T_m + \delta T_m)$

$$H^*(T) = \left(\rho c_p\right)_m \left[T - \left(T_m - \delta T_m\right)\right] + \Delta H^*\left(1 - F_s\right) \qquad (2.54)$$

23

F_s is the solid fraction rate, $F_s = \dfrac{T - T_m + \delta T_m}{2\delta T_m}$

Liquid Phase, $(T > T_m + \delta T_m)$

$$H^*(T) = (\rho c_p)_l \left[T - (T_m - \delta T_m) \right] + \rho \Delta H^* \qquad (2.55)$$

Equation 2.56 shows the dimensionless total enthalpy function with respect to non-dimensional temperature for solid, mushy and liquid phases.

$$H(\theta) = \begin{bmatrix} C_s \left[\theta - (\theta_m - \delta\theta_m) \right] & \theta < \theta_m - \delta\theta_m \\ C_m \left[\theta - (\theta_m - \delta\theta_m) \right] + \Delta H (1 - F_s) & \theta_m - \delta\theta_m \leq \theta \leq \theta_m + \delta\theta_m \\ C_l \left[T - (T_m - \delta T_m) \right] + \Delta H & \theta > \theta_m + \delta\theta_m \end{bmatrix} \qquad (2.56)$$

Dimensionless temperature θ is defined in Equation 2.57. This equation gives temperature formulation in terms of enthalpy for solid, mushy and liquid phases respectively.

$$\theta = \begin{bmatrix} h / C_{sl} + \theta_s & h < 0 \\ h / \left(0.5(1 + C_{sl})\right) + \theta_s & 0 \leq h \leq 0.5(1 + C_{sl})2\delta\theta \\ h - 0.5(1 + C_{sl})2\delta\theta + \theta_l & h > 0.5(1 + C_{sl})2\delta\theta \end{bmatrix} \qquad (2.57)$$

2.2.2.4 Temperature Transformation Method

Temperature transformation method developed by Cao & Fagri (1990) using advantages of enthalpy method and heat capacitance method. In this method phase change occurs in a temperature range unlike single temperature point. Phase change temperature range is accepted between $T_m - \delta T_m$ and $T_m + \delta T_m$. Non-dimensional form of energy equation for phase change model is described in Equation 2.40. Enthalpy formulations of the solid, liquid and mushy phases are indicated at Equation 2.58 to 2.61.

Solid Phase, ($T < T_m - \delta T_m$)

$$H^*(T) = 0 + \int_{T_{ref}}^{T} \rho_s c_{ps} dT + 0 \tag{2.58}$$

$$H^*(T) = (\rho c_p)_s \left[T - (T_m - \delta T_m) \right] \tag{2.59}$$

Mushy Phase, ($T_m - \delta T_m < T < T_m + \delta T_m$)

$$H^*(T) = (\rho c_p)_m \left[T - (T_m - \delta T_m) \right] + \rho \frac{\Delta H^*}{2 \delta T_m} \left[T - (T_m - \delta T_m) \right] \tag{2.60}$$

Liquid Phase, ($T > T_m + \delta T_m$)

$$H^*(T) = (\rho c_p)_l \left[T - (T_m - \delta T_m) \right] + \rho \Delta H^* \tag{2.61}$$

Dimensionless form of enthalpy formulation described in Equation 2.62.

$$H(\theta) = \begin{bmatrix} C_s \left[\theta - (\theta_m - \delta \theta_m) \right] & \theta < \theta_m - \delta \theta_m \\ \left(C_m + \dfrac{\rho \Delta H}{2 \delta \theta_m} \right) \left[\theta - (\theta_m - \delta \theta_m) \right] & \theta_m - \delta \theta_m \le \theta \le \theta_m + \delta \theta_m \\ C_l \left[T - (T_m - \delta T_m) \right] + \Delta H & \theta > \theta_m + \delta \theta_m \end{bmatrix} \tag{2.62}$$

Enthalpy can be written as $H = C(\theta)\theta + S(\theta)$ therefore specific heat C, source term S, and thermal conductivity K defined as a function of dimensionless temperature in Equation 2.63, 2.64 and 2.65.
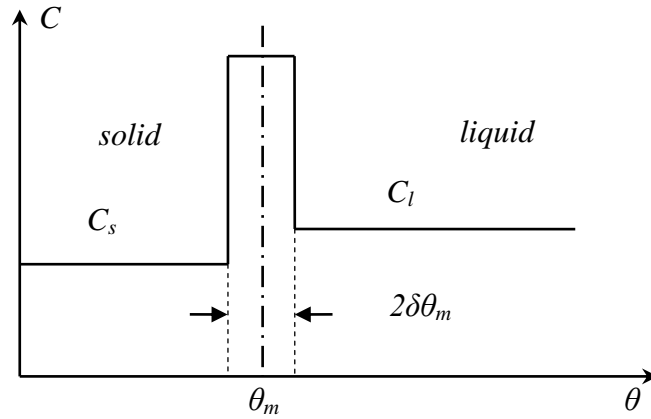
Figure 2.8 Specific heat temperature relationships

$$C(\theta) = \begin{cases} C_{sl} & \theta < \theta_m - \delta\theta_m \\ \dfrac{1}{2St\delta\theta} + \dfrac{1}{2}(1+C_{sl}) & \theta_m - \delta\theta_m \le \theta \le \theta_m + \delta\theta_m \\ 1 & \theta > \theta_m + \delta\theta_m \end{cases} \qquad (2.63)$$
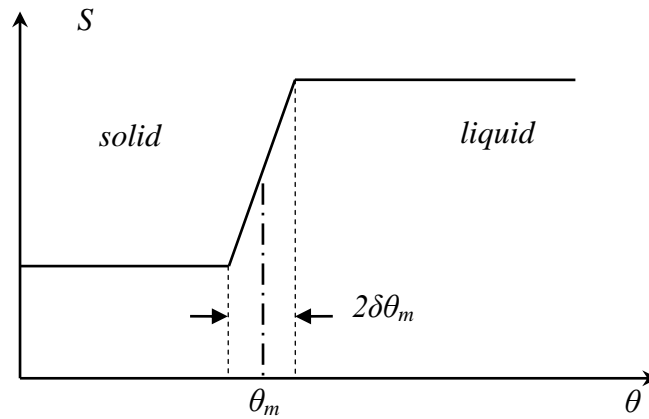
Figure 2.9 Source term temperature relationship

$$S(\theta) = \begin{cases} C_{sl}\delta\theta & \theta < \theta_m - \delta\theta_m \\ \dfrac{1}{2}(1+C_{sl})\delta\theta + \dfrac{1}{2St} & \theta_m - \delta\theta_m \le \theta \le \theta_m + \delta\theta_m \\ C_{sl}\delta\theta + 1/St & \theta > \theta_m + \delta\theta_m \end{cases} \qquad (2.64)$$

TTM has a significance role on calculating latent heat energy correctly. Energy equation described in terms of specific heat and source term. During the melting or solidification process, released or absorbed latent heat calculated in specific heat function and source term function.

$$K(\theta) = \begin{bmatrix} K_{sl} & \theta < \theta_m - \delta\theta_m \\ K_{sl} + (1 - K_{sl})(\theta_m + \delta\theta_m)/(2\delta\theta_m) & \theta_m - \delta\theta_m \leq \theta \leq \theta_m + \delta\theta_m \\ 1 & \theta > \theta_m + \delta\theta_m \end{bmatrix} \quad (2.65)$$

Phase change assumed occurring in a temperature range and thermal conductivity of the phase change material varies in different phases. Thermal conductivity of the PCM can be written as a function dependent of the temperature shown in Equation 2.65.

CHAPTER THREE
NUMERICAL ANALYSIS OF STEADY-STATE
NATURAL CONVECTION

Since the solid/liquid interface moves during the phase change process, the mathematical modeling of such a system becomes harder, especially for the case in the presence of natural convection effects. Although the pure conduction assumption makes the problem reasonable to simulate, it cannot meet the real case. It is known that the effective thermal conductivity (k_{eff}) approach is fairly adequate method to simplify the natural convection driven problems into pure conduction model. But for the case of melting or solidification, it would not be suitable to define a constant value of effective thermal conductivity. Especially for the inward melting the temperature difference between the moving interface and the outer surface is almost constant during the process. Hence, the influence of natural convection gradually increases with increasing the spacing between the shell and interface.

The main goal of the current study is to evaluate effective thermal conductivity inside spherical concentric capsules. In this study, we have carried out three different sets of numerical analyses. In the first step, the validity of the solution method of the steady-state analyses has been tested by commercial CFD software ANSYS-FLUENT regarding to the experimental data of Bishop (1966) for the case of air. As a second step, after the validation of the solution method steady-state natural convection of water is simulated for various geometrical shape and thermal conditions. As a result of this step, the effective thermal conductivity values are determined. At the last step, the correlated data is implemented into a numerical code (MATLAB) to simulate inward melting inside a spherical container, and the results are compared against the experimental measurements. Following sub-sections will define each problem and the related solution methods.

3.1 Effective Thermal Conductivity Evaluation

Natural convection problems can be also solved using effective thermal conductivity by assuming heat transfer occurred as conduction-controlled. However effective thermal conductivity evaluation has some restriction during the solidification and melting process of the phase change problems because interface position will move on over the time at the melting process. So, geometrical shape of the liquid region changes in time. In this situation different shape factors have been considered for the spherical geometries. For different shape factors natural convection effect changes so we should define variant effective thermal conductivity.

Heat transfer for evaluation of the effective thermal conductivity is defined in Equation 3.1 depending on the shape factor.

$$q = S'k_{eff}\Delta T \tag{3.1}$$

where S' is defined as shape factor. Shape factor for spherical coordinates is indicated in Equation 3.2 according to inner and outer radius of the sphere.

$$S' = \frac{4\pi}{\left(1/r_i\right)-\left(1/r_o\right)} \tag{3.2}$$

Effective thermal conductivity demonstration is defined in Equation 3.3.

$$k_{eff} = \frac{q}{\Delta T}\frac{\left(1/r_i\right)-\left(1/r_o\right)}{4\pi} \tag{3.3}$$

Effective thermal conductivity function is demonstrated in Equation 3.4 depending on spherical annulus ratio (L/r_i) of inward melting problem.

$$k_{eff} = a\left(L/r_i\right)^3 + b\left(L/r_i\right)^2 + c\left(L/r_i\right) + d \tag{3.4}$$

Different numerical analyses is carried out to evaluate effective thermal conductivity according to the temperature differences of the inner surface and outer surface (ΔT) and spherical annulus ratio (L/r_i).

3.2 Problem Definition of Steady-State Natural Convection of Inside Spherical Annulus

As a first step, the computational domain is modelled. As shown in the Figure 3.1, concentric sphere is considered to be two dimensional and axis-symmetrical. The inner and outer radius of the spherical annulus is indicated as r_i and r_o, respectively. The inner and outer surfaces are kept at constant temperature values as T_i and T_o, respectively.

Figure 3.1 Demonstration concentric sphere model
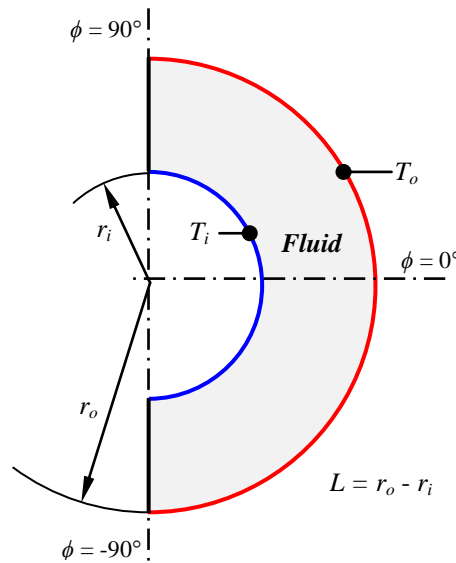
Different annulus ratios (L/r_i) are considered to validate the air flow pattern and temperature distributions using ANSYS-FLUENT software. Annulus ratio (spacing ratio) is defined as L/r_i. L is the differences of the inner and outer radius of the sphere. Spacing ratio $L/r_i = 0.67$, 1.00, 1.50 and 2.14 are determined according to Bishop (1966) experimental study.

Boundary condition of the considered model is determined as constant surface temperature. Outer surface temperature of the spherical capsule has higher temperature value. In the analyses, temperature differences are determined between outer surface and inner surface of the spherical model. This problem is used for validation of the solution method using different temperature differences as 25, 61 and 100°F.

For the each case of analyses, thermo-physical properties of the air except the density are defined to be constants and are obtained at a mean temperature, T_{mean} = $(T_o + T_i)/2$. Thermo-physical properties of the air are taken in air table of Incropera, DeWitt, Bergman, & Lavine (2006). The properties are stated according to mean temperature of the inner and outer surfaces in Table 3.1. Density of the air is calculated according to ideal gas law. It is identified as a function of temperature which is valid for the temperature range considered in this study as;

$$\rho_{air} = 1\text{E-05}T^2 - 0.0104\text{T} + 3.3209 \tag{3.5}$$

Table 3.1 Thermo-physical properties of air

T_{mean}	ρ	c_p	k	μ	v	β
6.95 ^{o}C (12.5 ^{o}F)	1.10192	1007.71	0.02762	1.93E-05	1.77E-05	0.003146
16.95 ^{o}C (30.5 ^{o}F)	1.06864	1008.11	0.02836	1.98E-05	1.87E-05	0.003050
27.78 ^{o}C (50 ^{o}F)	1.03259	1008.55	0.02916	2.03E-05	1.98E-05	0.002952

As a second step, the geometric model of the previous section is considered similarly for this section. However, water is used for as fluid instead of air between the two concentric spheres.

Different types of annulus ratios are considered to calculate the total heat transfer using ANSYS-FLUENT software. Total heat transfer is used to calculate effective thermal conductivity for related annulus ratio and temperature differences. Annulus ratio (spacing ratio) is defined L/r_i. L is the differences of the inner and outer radius of the sphere. Annulus ratio L/r_i = 0.67, 1.00, 1.50 and 2.14 are determined similarly according to previous study.

As a boundary condition, inner and outer surfaces are defined constant temperatures. Outer surface temperature of the spherical capsule is higher temperature value. In the analyses, initial temperature surface of the inner sphere is taken to be 0°C. Surface temperature of the outer sphere is determined 2°C, 4°C, 8°C, 12°C and 24°C. The reason of the determining low temperature is that to investigate the effect of the density inversion at 4°C. The density value of the water becomes maximum at 4°C temperature value.

Thermo-physical properties of the water are obtained using mean temperature of the inner and outer surfaces. According to mean temperature, thermal-physical properties of water are identified using Incropera at al. (2006) and these value are shown in Table 3.2. Density of water is defined as a function of mean temperature which is shown in Equation 3.6. (Seybert & Evans, 2005).

$$\rho_{water} = -0.007085T^{2} + 3.925T + 456.49 \tag{3.6}$$

Table 3.2 Thermo-physical properties of water

T_{mean}	ρ	c_p	k	μ	ν	β
1 $^{\circ}$C	999.99133	4214.23	0.5709	1.70E-03	1.70E-06	6.5E-05
2 $^{\circ}$C	999.99725	4211.45	0.5730	1.65E-03	1.65E-06	6.2E-05
4 $^{\circ}$C	1000.0898	4205.91	0.5770	0.0015585	1.56E-06	5.5E-05
6 $^{\circ}$C	1000.0570	4200.36	0.5804	0.0014627	1.46E-06	4.9E-05
12 $^{\circ}$C	999.55913	4188.35	0.5910	0.0012062	1.21E-06	1.2E-05

3.3 Solution Methods of the Model

The governing equations are discretized into algebraic sets of equations with using Control-Volume-Approach of Patankar (1980). Power-Law scheme is implemented for evaluating the values at the control surfaces for each transport parameter. SIMPLE algorithm is used as a solution algorithm of governing equations. All the solution methods that used in commercial CFD software ANSYS-FLUENT, are explained clearly in this section.

Considering the incompressible, two-dimensional, steady-state and laminar flow inside a spherical annulus, governing equations can be reduced as

Continuity

$$\frac{\partial u}{\partial x_i} = 0 \tag{3.7}$$

Momentum

$$\frac{\partial}{\partial x_j}\left(\rho u_i u_j\right) = \mu \frac{\partial^2 u_i}{\partial x_j \partial x_j} - \frac{\partial p}{\partial x_i} + \rho g_i \tag{3.8}$$

Energy

$$\frac{\partial}{\partial x_i}\left(\rho u_i h\right) = \frac{\partial}{\partial x_i}\left(k \frac{\partial T}{\partial x_i}\right) \tag{3.9}$$

The computational domain is considered half of sphere as axis-symmetrical boundary condition and divided by 150.000 control volume. Figure 3.2 indicates the computational domain and mesh structure. Because of the higher temperature and velocity gradient at surfaces of the sphere, mesh density is increased near the inner and outer surfaces.
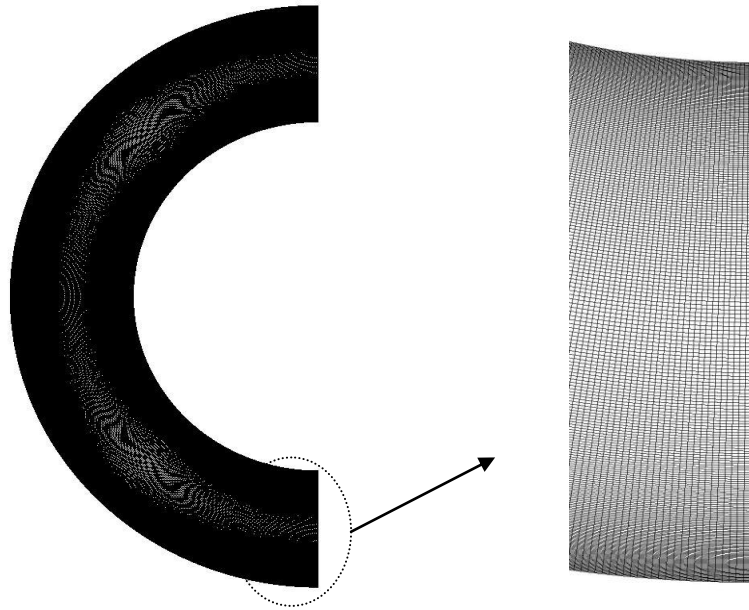
Figure 3.2 Computational domain and mesh demonstration

CHAPTER FOUR
EXPERIMENTAL STUDY

4.1 Experimental Investigation Inward Melting and Solidification of Water

In the evaluation of the effective thermal conductivity, the problem is reduced into two-dimensional, steady-state problem without phase change. Hence, the convenience of these simplifications is revealed regarding to the experimental comparisons. The main purpose of the experimental studies is the verification of the numerical codes which is integrated effective thermal conductivity function. Validation of the effective thermal conductivity evaluation is tested according to this experimental study.

4.2 Experimental Setup

In the experiments, a spherical capsule is used with an inner diameter and wall thickness of 55 mm and 2 mm, respectively. POLSCIENCE constant temperature bath is used to keep constant of the surface temperature of the spherical capsule. In order to obtain homogenous temperature distribution at the beginning, spherical capsule which have 40% ethylene-glycol water mixture is submerged into the constant temperature bath. Spherical capsule is filled with distilled water but top of the capsule is kept for air by volume %10. The space is kept for air is volume change during the solidification.

Thermo-physical properties of the heat transfer fluid ethylene-glycol water mixture are obtained from ASHRAE (2001).

Table 4.1 Thermo-physical properties of HTF

T_{mean}	ρ	c_p	k	μ	v	β
12°C	1057.6	3485	0.419	2.57E-03	2.43E-06	0.00065
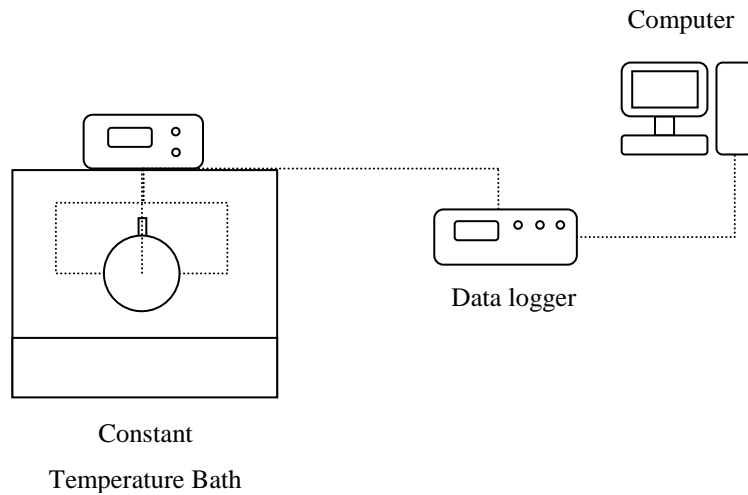
Figure 4.1 Schematic view of the experimental setup

4.3 Measurement Method

As a measurement method in the experiment is consist of three T-type thermocouples. One of the thermocouple is placed centre of the capsule. Thermocouple is fixed in the centre by the help of the sticks so during the solidification location of the thermocouple can not slip. During the melting of the water, the ice cannot move in the spherical capsule. Therefore, this kind of melting process is called as constrain melting. The other thermocouples are placed surface of the spherical capsule with the equal angle.
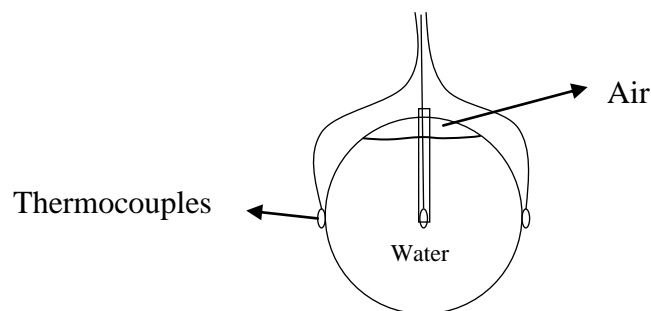
Figure 4.2 Thermocouple locations inside sphere

Thermocouples locations are demonstrated schematically in Figure 4.2. T-type thermocouples consist of two copper and constantan wires. T-type thermocouple is

36

suitable for temperature range of -270 to 350°C. The accuracy of the T-type thermocouple is nearly ±1°C. During the experiment, temperature data is taken using Agilent 34970A data logger. This data logger has 20 two-wire ports. Experimental data is obtained every ten seconds.

Figure 4.3 Experimental setup and spherical capsule demonstration

CHAPTER FIVE
RESULTS AND DISCUSSION

Enthalpy method (EM) and temperature transformation method (TTM) are used in the phase change problem solutions. The non-dimensional values of the phase change problem are described in Table 5.1.

Table 5.1 Non-dimensional initial values of problem

Surface temperature, T_o	-0.7
Initial temperature, T_i	0.3
Phase change temperature, T_m	0
Specific heat, C_{sl}	1
Thermal conductivity, K_{sl}	1
Stefan number, Ste	0.33

In the validation and comparison of these methods the same non-dimensional parameters are taken.

The difficulty of the phase change problems is having non-linear features of the equations. Therefore in order to evaluate temperature or enthalpy values of the control volume, iterative solution is needed. In the numerical code temperature and enthalpy values are controlled every iteration and ensured converging 10^{-13}. Also energy balance is assuring every time step.

5.1 Validation of the Enthalpy Method

The validation of enthalpy method is controlled using analytical solution of the one dimensional for semi-infinite phase change problem Özışık (1993). Different number of control volume is considered and divided by 10, 50, 500 and 5000 control volume. Numerical solution of the enthalpy method is evaluated MATLAB software. Evaluated temperature values of the each control volume compared with analytical solution. Table 5.2 shows the analytical solution and temperature distribution of the enthalpy method for different grid number.

Table 5.2 Temperature distribution of the enthalpy method

X	Analytical Solution	Enthalpy Method			
		Temperature Δx=0.1	Temperature Δx=0.02	Temperature Δx=0.002	Temperature Δx=0.0002
0	-0.7	-0.7	-0.7	-0.7	-0.7
0.1	0.0872	0.0111	0.0812	0.0883	0.088
0.2	0.2302	0.1739	0.2266	0.2302	0.2302
0.3	0.285	0.2608	0.2833	0.2845	0.2846
0.4	0.2979	0.2905	0.2973	0.2976	0.2977
0.5	0.2998	0.2981	0.2997	0.2998	0.2998
0.6	0.3	0.2997	0.3	0.3	0.3
0.7	0.3	0.3	0.3	0.3	0.3
1	0.3	0.3	0.3	0.3	0.3

Temperature Distribution (Δτ=0.0002;τ=0.01)

Temperature distribution of the enthalpy method calculated for $\Delta\tau = 0.0002$ dimensionless time step until $\tau=0.01$ dimensionless time. According to Table 5.2, increasing grid number of the enthalpy method gives better result comparing with analytical solution.

Table 5.3 Interface location of the enthalpy method

τ	Analytical Solution	Enthalpy Method			
		Δx=0.1	Δx=0.02	Δx=0.002	Δx=0.0002
0.001	0.0187	0.1	0.04	0.02	0.0186
0.002	0.0264	0.1	0.04	0.028	0.0264
0.003	0.0324	0.1	0.04	0.034	0.0324
0.004	0.0374	0.1	0.04	0.038	0.0374
0.005	0.0418	0.1	0.06	0.044	0.042
0.006	0.0458	0.1	0.06	0.048	0.046
0.007	0.0495	0.1	0.06	0.05	0.0496
0.008	0.0529	0.1	0.06	0.054	0.053
0.009	0.0561	0.1	0.06	0.056	0.0564
0.01	0.0591	0.1	0.08	0.06	0.0594

Interface Location (Δτ=0.0002;τ=0.01)

The validation of the interface position is also calculated using MATLAB software. Interface position of the enthalpy method is calculated for different grid number as 10, 50, 500 and 5000. Increasing control volume gives better result with

analytical solution. Dimensionless time step is taken $\Delta\tau = 0.0002$ and the solution is calculated at τ=0.01.
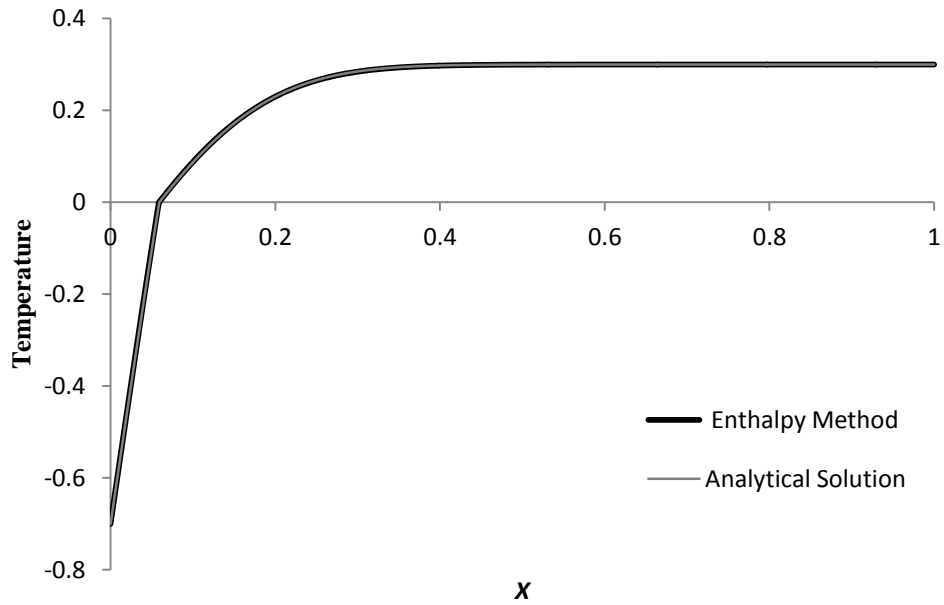

Figure 5.1 Temperature distribution of enthalpy method for τ=0.01

Figure 5.1 shows that temperature distribution of at an instant time. Enthalpy method and analytical solution compared with respect to dimensionless length.
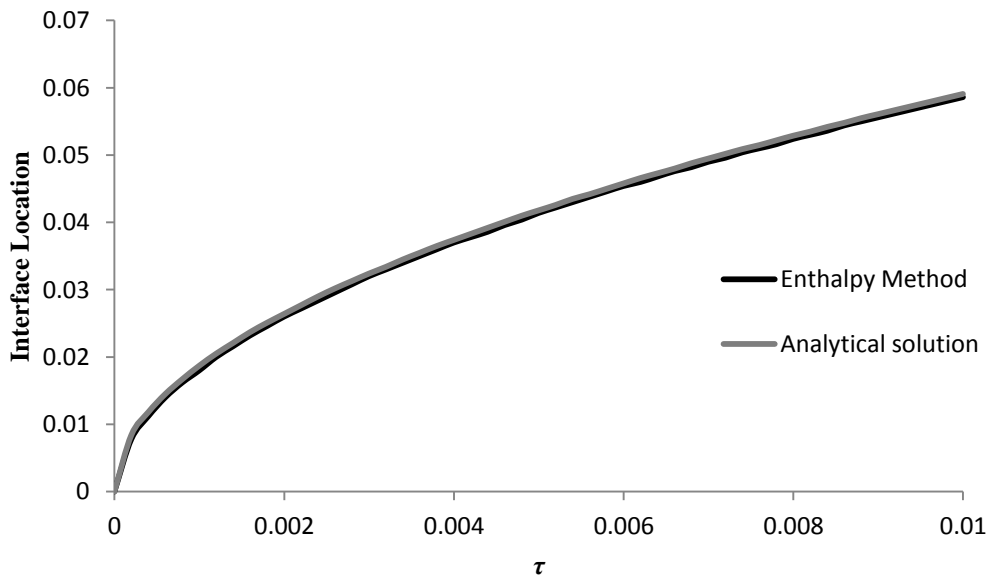

Figure 5.2 Interface location of the enthalpy method for τ=0.01

Figure 5.2 demonstrate the interface movement of the phase change problem in cartesian coordinates. Also comparing interface location of the PCM with the analytical solution proves the accuracy of this method. After total calculating time $\tau=0.01$, six percent of solidification of the phase change materials is completed.

5.2 Validation of the Temperature Transformation Method

The temperature transformation method developed by Faghri (1990) is calculated using boundary values of Table 5.1. The same number of control volume with the enthalpy method is used in this method. Each temperature values and interface location at control volumes is controlled with analytical solution. Table 5.4 indicates the temperature distribution of the temperature transformation method according to dimensionless length.

Table 5.4 Temperature distribution of the temperature transformation method

		Temperature Distribution ($\Delta\tau=0.0002;\tau=0.01$)			
		Temperature Transformation Method			
X	**Analytical Solution**	**Temperature $\Delta x=0.1$**	**Temperature $\Delta x=0.02$**	**Temperature $\Delta x=0.002$**	**Temperature $\Delta x=0.0002$**
0	-0.7	-0.7	-0.7	-0.7	-0.7
0.1	0.0872	-0.1503	0.0802	0.0872	0.0877
0.2	0.2302	0.1642	0.2374	0.23	0.23
0.3	0.285	0.2675	0.2884	0.2845	0.2844
0.4	0.2979	0.2931	0.2984	0.2977	0.2976
0.5	0.2998	0.2987	0.2999	0.2998	0.2998
0.6	0.3	0.2998	0.3	0.3	0.3
0.7	0.3	0.3	0.3	0.3	0.3
1	0.3	0.3	0.3	0.3	0.3

Table 5.4 also shows the temperature values of the increasing grid number of the method. The comparison with the analytical method is demonstrated and the solution of the method gives better result increasing the number of grid.

Table 5.5 Interface location of the temperature transformation method

Interface Location (Δτ=0.0002;τ=0.01)					
τ	Analytical Solution	Temperature Transformation Method			
		Δx=0.1	Δx=0.02	Δx=0.002	Δx=0.0002
0.001	0.0187	0.1	0.04	0.02	0.0184
0.002	0.0264	0.1	0.06	0.028	0.0262
0.003	0.0324	0.1	0.06	0.034	0.0322
0.004	0.0374	0.1	0.06	0.038	0.0372
0.005	0.0418	0.2	0.06	0.044	0.0418
0.006	0.0458	0.2	0.08	0.048	0.0458
0.007	0.0495	0.2	0.08	0.05	0.05
0.008	0.0529	0.2	0.08	0.054	0.0528
0.009	0.0561	0.2	0.08	0.058	0.056
0.01	0.0591	0.2	0.08	0.06	0.059

Table 5.5 present the interface location of the temperature transformation method. Analytical solution of the interface positions are calculated with respect to dimensionless time. Δx=0.002 and Δx=0.0002 values of the interface location are very close to each other. The comparison of the interface location with analytical solution proves the accuracy of this method.

0.4
0.2
0
-0.2
-0.4
-0.6
-0.8
0
0.2
0.4
0.6
0.8
1
Temperature
Length
Analytical Solution
TTM

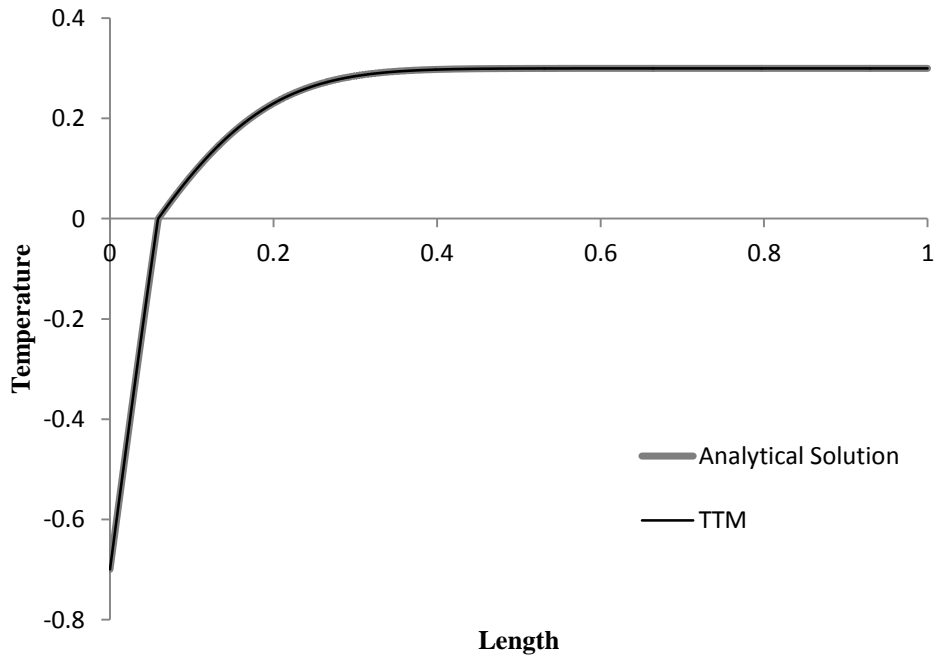

Figure 5.3 Temperature distribution of temperature transformation method for τ=0.01

The Figure 5.3 demonstrates the comparison between analytical solution and temperature transformation method. At the dimensionless time $\tau = 0.01$, temperature distribution of this method is presented with respect to dimensionless length.
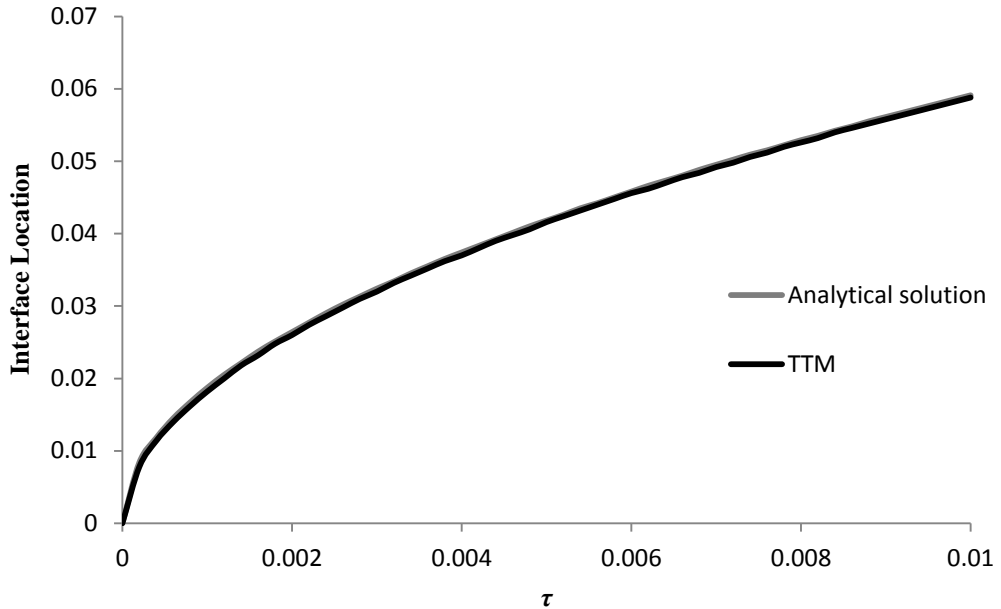
Figure 5.4 Interface location of the temperature transformation method for $\tau=0.01$

Interface location distribution of the temperature transformation method is demonstrated in Figure 5.4. With respect to dimensionless time evaluated interface positions are compare to analytical solution.

5.3 Comparison of the E.M and T.T.M with Analytical Method

The comparison of the enthalpy method and temperature transformation method with analytical solution is to determine the suitable method for phase change problems. Comparison of the methods is investigated temperature accuracy, interface position and solution time of the MATLAB code.

Figure 5.5 shows that temperature distribution of the EM, TTM and analytical solution according to dimensionless length. The biggest error occurs nearby the phase change point for phase change problem. When the figure is zoomed in nearby

the phase change point, TTM gives more accurate results with analytical method according to EM.
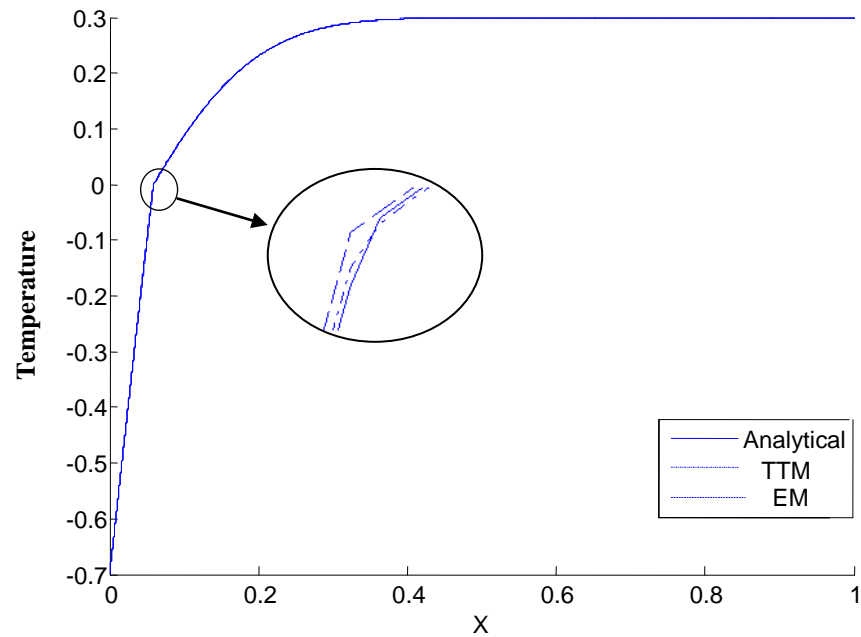

Figure 5.5 Temperature comparisons of the methods

Also the comparison of the methods for interface location is indicated in Figure 5.6. Analytical solution, EM and TTM solutions are zoomed in the figure and TTM is the more accurate than the other method.
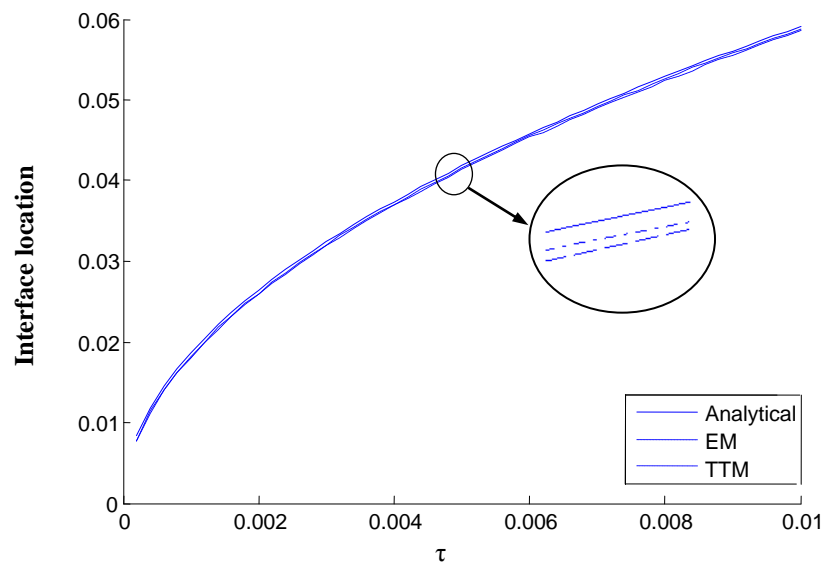

Figure 5.6 Interface position comparisons of the methods

44

Another comparison for numerical errors is calculated for specified time step and grid distance. Dimensionless temperature of each node is determined for both EM and TTM. The error of the specified nodes is computed from temperature of the methods and analytical solution. The highest percent error is occurred at phase change temperature point. But comparing the numerical methods between them, TTM gives lower percent error at each node.

Table 5.6 Comparison of the numerical methods in different grid number

Numerical Method Comparison Δτ=0.0002;Δx=0.002; τ=0.01					
X	Analytical Solution	Enthalpy Method		Temperature Transformation Method	
		Temperature	% Error	Temperature	% Error
0	-0.7	-0.7	0	-0.7	0
0.04	-0.2191	-0.2122	3.149247	-0.2166	1.14103
0.06	0.002	0.0035	75	0.0008	60
0.1	0.0872	0.0883	1.261468	0.0872	0
0.2	0.2302	0.2302	0	0.23	0.08688
0.3	0.285	0.2845	0.175439	0.2845	0.17544
0.4	0.2979	0.2976	0.100705	0.2977	0.06714
0.5	0.2998	0.2998	0	0.2998	0
0.6	0.3	0.3	0	0.3	0
0.7	0.3	0.3	0	0.3	0
1	0.3	0.3	0	0.3	0

The other comparison of the numerical methods is the solution time. Table 5.7 shows two numerical methods solution time in different node number. Every dimensionless time step, the solution time is calculated for both TTM and EM. Increasing node number is caused the increment of the solution time. But comparison of the numerical methods at the same node number, TTM has a faster solving capacity.

Table 5.7 Comparisons of the solution time in different grid number

Dimensionless Time	Enthalpy Method N=10 (s)	Temperature Transformation Method N=10 (s)	Enthalpy Method N=500 (s)	Temperature Transformation Method N=500 (s)
0.001	0.1066	0.0924	4.1152	3.6165
0.002	0.1071	0.0902	4.079	3.6059
0.003	0.107	0.0898	4.2465	3.6139
0.004	0.1071	0.0911	4.1802	3.6254
0.005	0.1068	0.0947	4.0362	3.6036
0.006	0.1077	0.0894	4.1422	3.6229
0.007	0.1068	0.0889	4.0906	3.6142
0.008	0.1073	0.0892	4.0248	3.6063
0.009	0.1087	0.0892	4.0882	3.631
0.01	0.1071	0.0909	4.8392	3.5978

5.4 Parametric Study

Comparative study described above is demonstrated the numerical solution method. Temperature transformation method gives the better result for phase change problems. In this section parametric study of the TTM is achieved according to Bi number change and Stefan number change. Stefan number is described as ratio of sensible heat of the fluid phase to latent heat, $\mathrm{Ste} = c_L\left(T_{in} - T_m\right)/\Delta h$. Bi number is defined ratio of the surface convection resistance to diffusion resistance in the PCM, $\mathrm{Bi} = hL/k_l$. In the subsection Stefan change and Bi number change of the TTM is demonstrated.

5.4.1 Stefan Number Variation

In this part of study different Stefan number variation is considered. The thermal properties of the numerical analysis are described below the Figure 5.7. Ste=0.01, 0.1, 1.00 and 3.00 values Stefan number take in account in numerical analysis. Increasing Stefan number, at an instant time phase change point is increasing and energy change of PCM is mostly occurred as sensible heat.

Figure 5.7 Stefan number effect upon temperature distributions ($\tau = 3.2e^{-3}$, $\theta_m = 0$, $\theta_i = 0.1$, $\theta_o = -0.9$, $C_{sl} = 0.4$, $K_{sl} = 3.8$)

The interface position change is also indicated in Figure 5.8. The increasing Stefan number effects the interface position and at the same time interface movement of the PCM is accelerating.
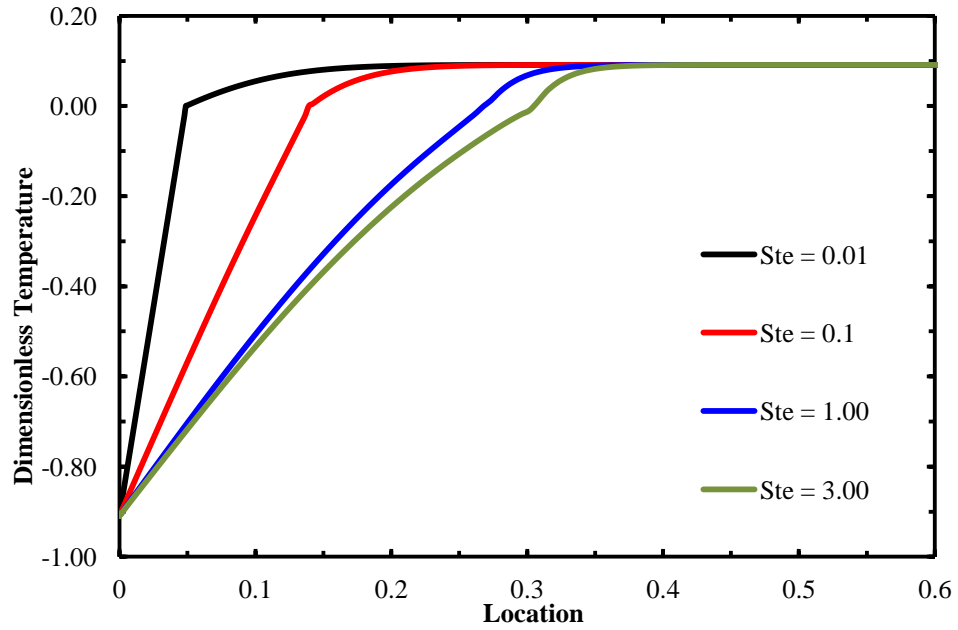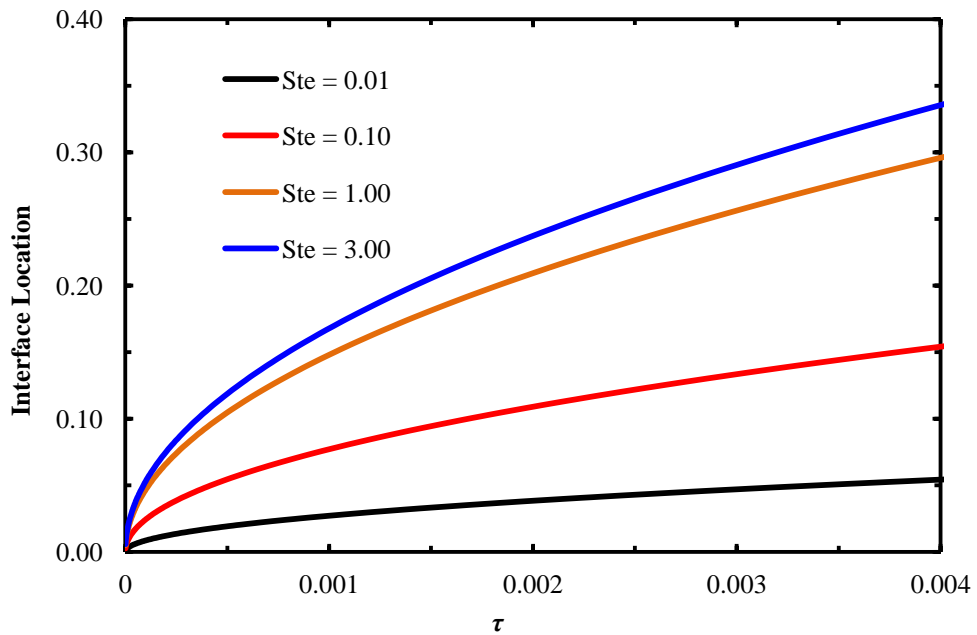

Figure 5.8 Stefan number effect upon interface position ($\tau = 3.2e^{-3}$, $\theta_m = 0$, $\theta_i = 0.1$, $\theta_o = -0.9$, $C_{sl} = 0.4$, $K_{sl} = 3.8$)

5.4.2 Biot Number Variation

This part of study unlike the constant surface temperature, convection heat transfer considered at surface for cartesian coordinate. Bi number is considered in different values in numerical analysis. In Figure 5.9 dimensionless temperature distribution is shown for different Bi number (1, 10, 20, 50 and 100). Increment of the Bi number is causing increasing convection heat transfer from surface so dimensionless surface temperature decreases approximate 0.05 to -0.35.
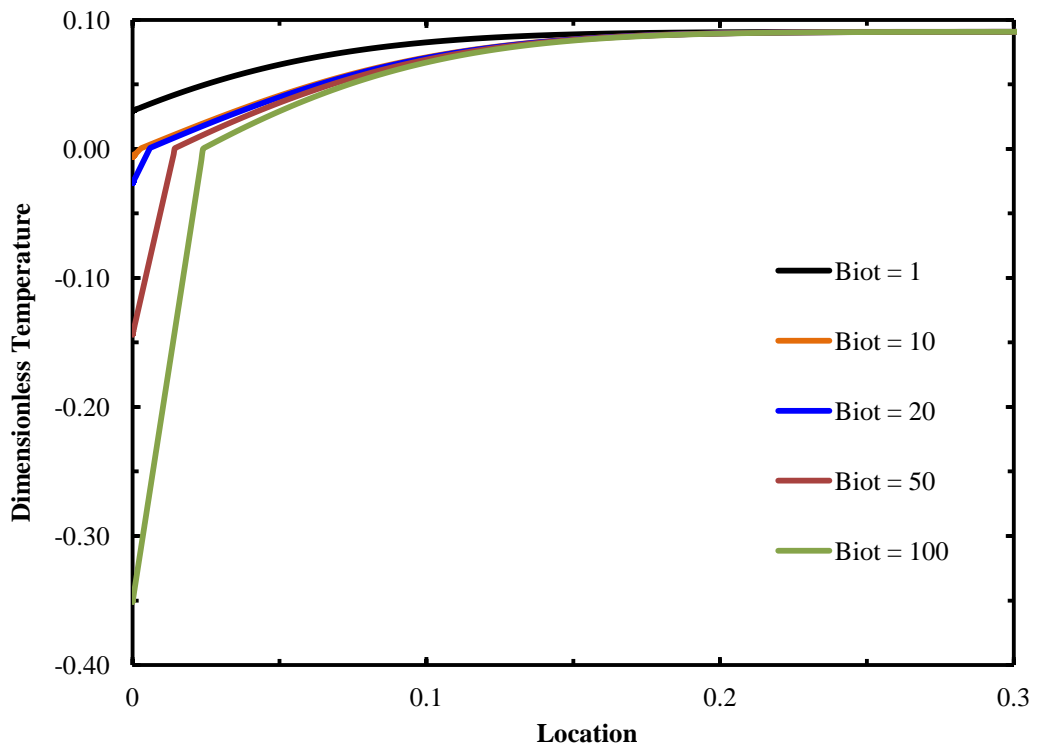
Figure 5.9 Biot number effect upon temperature distributions ($\tau = 3.2\mathrm{e}^{-3}$, Ste = 0.01, $\theta_m = 0$, $\theta_i = 0.1$, $\theta_{inf} = -0.9$, $C_{sl} = 0.4$, $K_{sl} = 3.8$)

Figure 5.10 indicate the interface movement at the variable Bi number. The Bi number increment is causing speed up the heat transfer in the PCM. Therefore interface position is increasing for higher Bi number. Surface temperature for Bi=1 doesn't lower the phase change temperature so interface movement cannot occur.
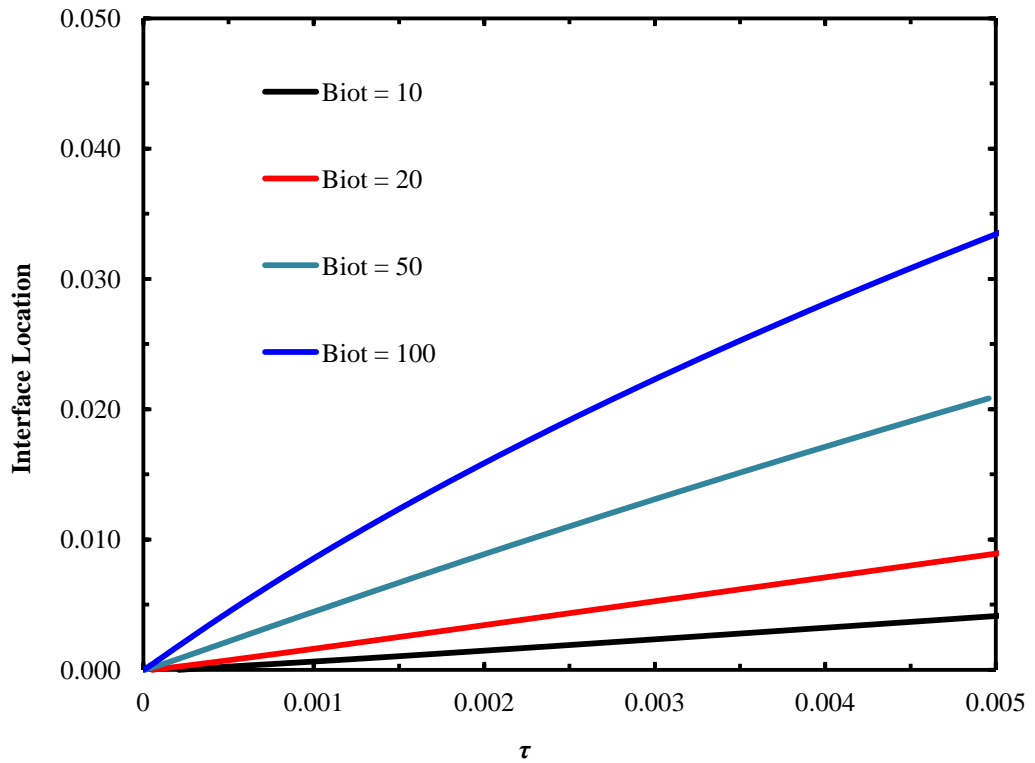
Figure 5.10 Biot number effect upon interface position ($\tau = 3.2\mathrm{e}^{-3}$, $\theta_m = 0$, $\theta_i = 0.1$, $\theta_o = -0.9$, $C_{sl} = 0.4$, $K_{sl} = 3.8$)

5.5 Validation of the Steady State Natural Convection Inside Sphere

Numerical methodology is introduced with reproducing the experimental study of Bishop (1966). Bishop and his colleagues took into account natural convection of air inside spherical annulus with isothermal surfaces. In the experimental study, Bishop varied the spacing ratio (L/r_i) to be 0.19, 0.67, 1.00, 1.50 and 2.14. The temperature difference (T_o - T_i), on the other hand, was changed between 8.33°C (15°F) to 55.55°C (100°F). Comparative results are obtained in terms of the average Nusselt number and the flow patterns.

Bishop suggested the following correlation for natural convection of air inside annulus,

$$\mathrm{Nu} = 0.332\mathrm{Gr}^{0.270}\left(L/r_i\right)^{0.517} \tag{5.1}$$

On the other hand, in order to compare Nusselt number, different set of numerical analyses have been achieved for air and described briefly in chapter 3.2. Different annulus ratio and temperature differences are considered to evaluate total heat transfer. Total heat transfer evaluated from numerical analyses is used to calculate average Nusselt number shown in Equation 5.2.

$$Nu = \frac{qL}{4\pi k (\Delta T) r_i^2}$$
(5.2)

where q is the heat transfer from inner or outer surface of the sphere.

Table 5.7 Comparison of Nusselt Number

Annulus Ratio	ΔT	Nusselt Number		Difference
		Eq. (5.1)	Numerical Results	
(L/r_i)	(°C, °F)	(-)	(-)	(%)
	13.89,(25)	7.06	6.99	1.0
0.67	33.89,(61)	8.64	8.38	3.1
	55.56,(100)	9.50	9.11	4.1
	13.89,(25)	10.43	10.11	3.1
1.00	33.89,(61)	12.77	12.05	5.6
	55.56,(100)	14.03	13.10	6.7
	13.89,(25)	14.91	14.21	4.7
1.50	33.89,(61)	18.26	16.95	7.2
	55.56,(100)	20.06	18.43	8.1
	13.89,(25)	19.90	18.90	5.0
2.14	33.89,(61)	24.37	22.50	7.8
	55.56,(100)	26.77	24.42	8.8

Comparative results are represented in Table 5.7 for various spacing ratios and temperature differences. Increasing spacing factor or temperature tends to increase the surface Nusselt number. It is also clear that for higher spacing ratios or temperature differences, the difference between the predicted and the experimental data increases. In the experiments, there may be three-dimensional flow patterns or turbulence effects may occur especially for higher Grashof numbers, which are not considered in the current mathematical model. Nevertheless, the predicted results

have reasonable consistency with the results of reference work and the maximum deviation is found to be less than 9%.
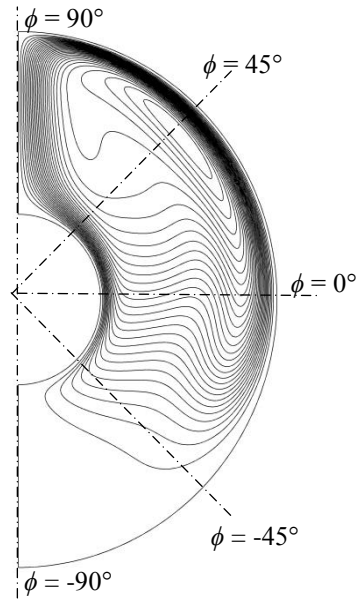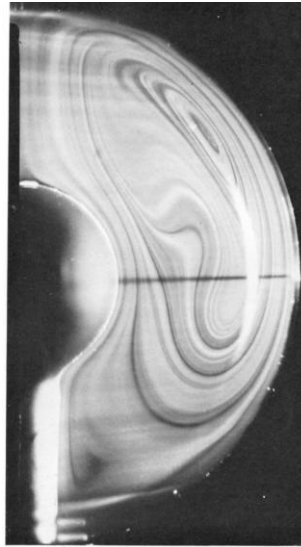
(a) L/r$_i$ = 2.14, ΔT = 13.89°C (25°F)
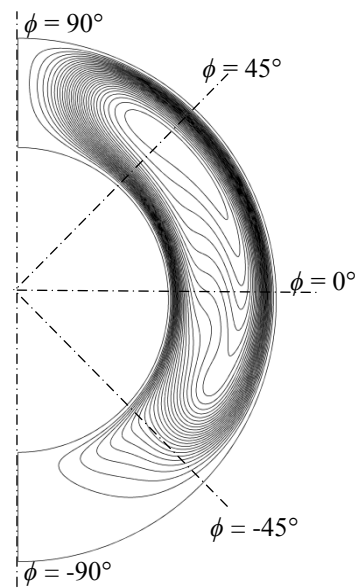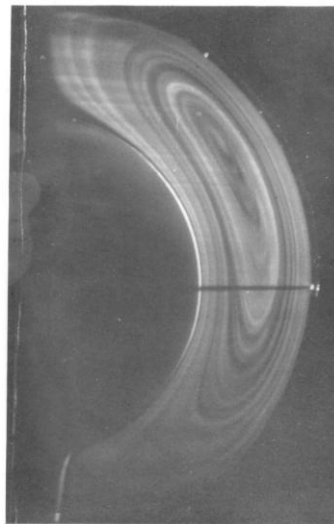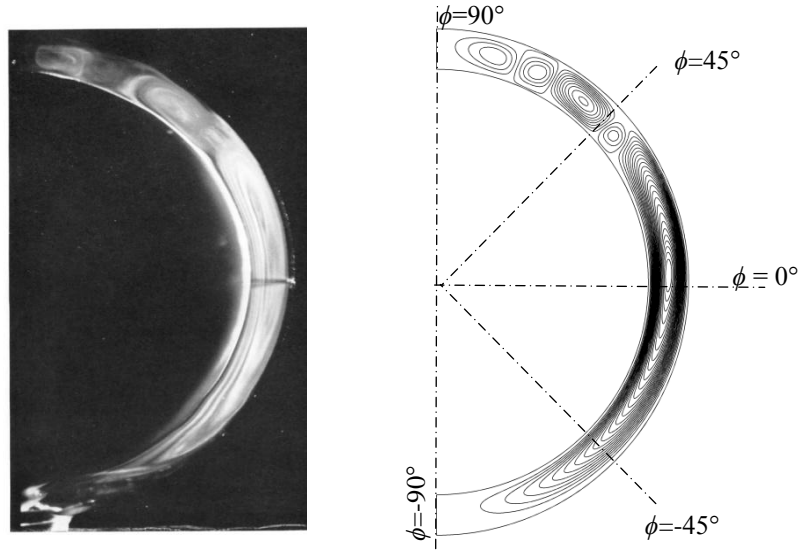

(b) L/r$_i$ = 0.72, ΔT =8.33°C (15°F)

(c) L/r$_i$ = 0.19, ΔT = 8.33°C (15°F)

Figure 5.11 Airflow patterns

Bishop indicated that three distinct flow patterns were observed namely, *kidney-shaped-eddy*, *crescent-eddy*, and *falling-vortices*. In Figure 5.11, these three flow patterns are compared against the flow visualizations of the reference work. In Figure 5.11(a), flow patterns are represented for L/r_i = 2.14. A distortion is observed close to $\phi = 0°$ line for the experimental observations and the shape of the flow pattern looks like a *kidney*. However, the predicted flow pattern does not resemble with the experimental one especially for -45° < ϕ < 45°. As can be seen in Table 1, this discrepancy induces a deviation of 5% in terms of the surface Nusselt number. On the other hand, as seen in Figure 5.11(b), for L/r_i = 0.72, the domain is dominated by a big circulation cell and the shape is similar to the *crescent*. The center of the circulation cell is observed for 0° < ϕ < 45° as in the reference work. In Figure 5.11(c) patterns are given for L/r_i = 0.19. Since the spacing is so small for this configuration, at the top of the annulus, 40° < ϕ < 90°, small vortices are observed, and this type of flow patterns is called as *falling vortices*. On the other hand, crescent type flow pattern is dominated for the rest of the domain for -90° < ϕ < 40°. Comparative results reveal that the numerical method that is used in the current work has a reasonable consistency with experimental findings.

52

5.6 Evaluation of Effective Thermal Conductivity

During the inward melting process, the interface will move from the outer surface through the center of the sphere. Here, we have calculated the effective thermal conductivity for several annulus ratios and temperature differences to evaluate a correlation that can be used in simplified numerical codes for inward melting. The thermal and geometric parameters that are used to evaluate effective thermal conductivity are listed in Table 5.8. In the analyses, the temperature of the inner sphere is kept constant at the phase change temperature of water, at 0°C.

Table 5.8 Parameters for steady-state natural convection of water

L/r_i	0.67, 1.00, 1.50 and 2.14
$T_i - T_o$ (°C)	2, 4, 8, 12 and 24

In Figure 5.12, for L/r_i = 0.67 isotherm and streamline distributions are demonstrated three different surface temperature T_o = 2°C, 8°C and 12°C respectively. Surface temperature, T_o = 2°C density of water is increasing and reaches the higher degree, the cold water inside the sphere moves through the top of the sphere. Therefore, while velocity distribution moves upwards inner surface of the sphere, the movement on the outer surface tends to downwards. Consequently clock-wise circulation takes place for this region. But two different circulation movement occurs for T_o = 8°C. While the high density hot water located outer surface of the sphere is moving downward of the sphere, the cold water tends to move inner sphere to top of the sphere. In this region counter clock-wise circulation is formed. The other velocity movement occurs clock-wise circulations because of the density change at 4°C. In Figure 5.12(b), Two different circulations have been formed for T_o = 8°C. The small circulation occurred inner sphere between 0° < ϕ < -90°. In Figure 5.12(c) at the bottom of the sphere ϕ = -90° because of the higher temperature differences between sphere surfaces.

(a) $T_o = 2°C$

(b) $T_o = 8°C$

(c) $T_o = 12°C$
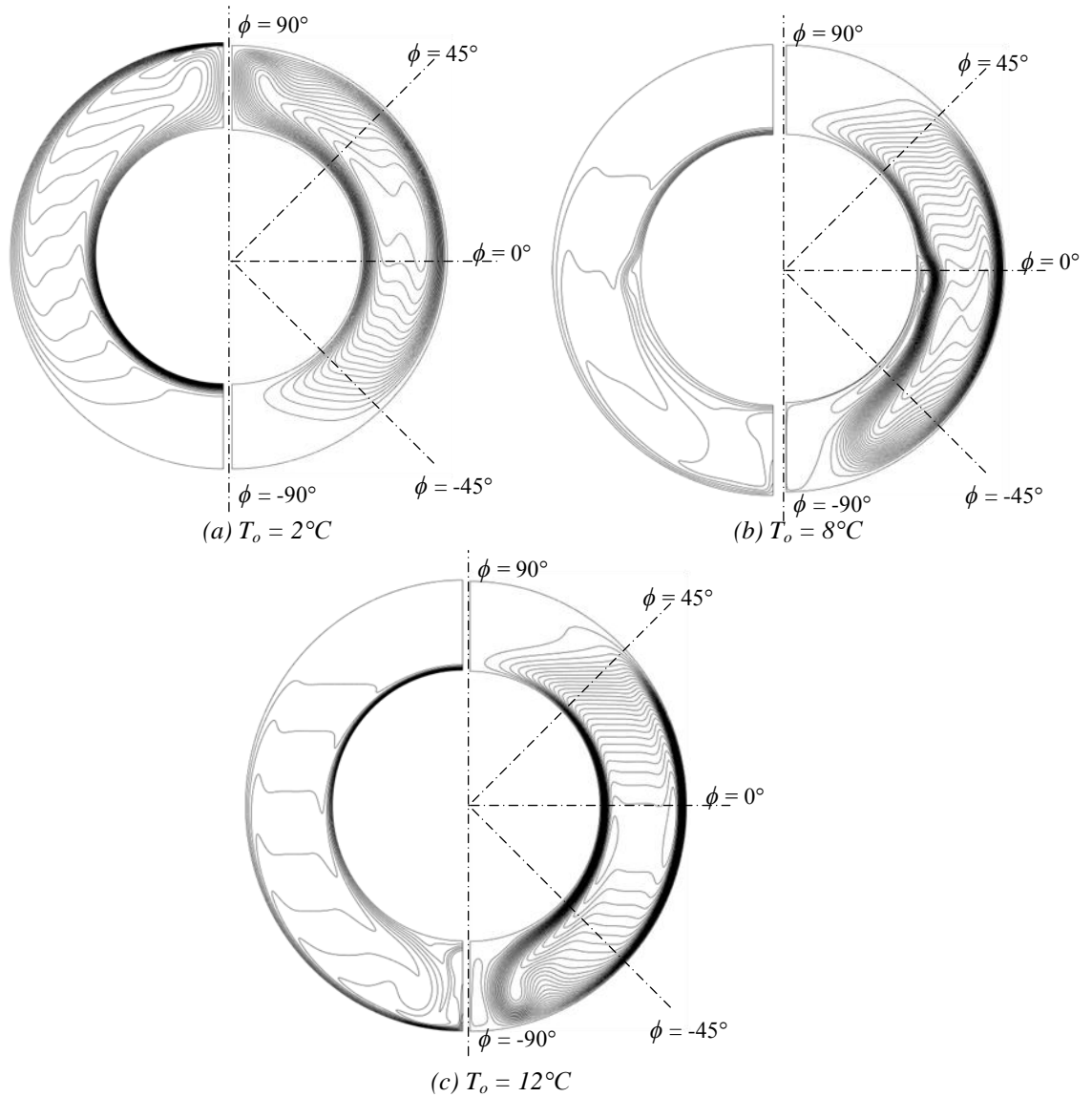
Figure 5.12 Temperature and velocity distribution for $L/r_i = 0.67$

Increasing spacing ratios in Figure 5.13(a) and Figure 5.14(a) thermal stratification have been occurs through the below the computational domain ($0° < \phi < -90°$). For surface temperature $T_o = 2°C$, circulation moves upper side of the computational domain. But as shown in Figure 5.13(b,c) and Figure 5.14(b,c) thermal stratification occurs upper side of the computational domain ($0° < \phi < 90°$) and circulation slide through the bottom of the concentric spheres. Consequently, inner circulation cell is formed below the computational domain in a narrow range.

Increasing the surface temperature of the sphere effects the natural convection so as seen in Figure 5.13(c) and Figure 5.14(c), secondary circulation cell is occurred bottom side of the sphere. Besides for higher spacing ratios, it is clear that a jet-flow forms at the bottom of the inner sphere and hits on the outer surface at $\phi = -90°$.

(a) $T_o = 2°C$

(b) $T_o = 8°C$

(c) $T_o = 12°C$
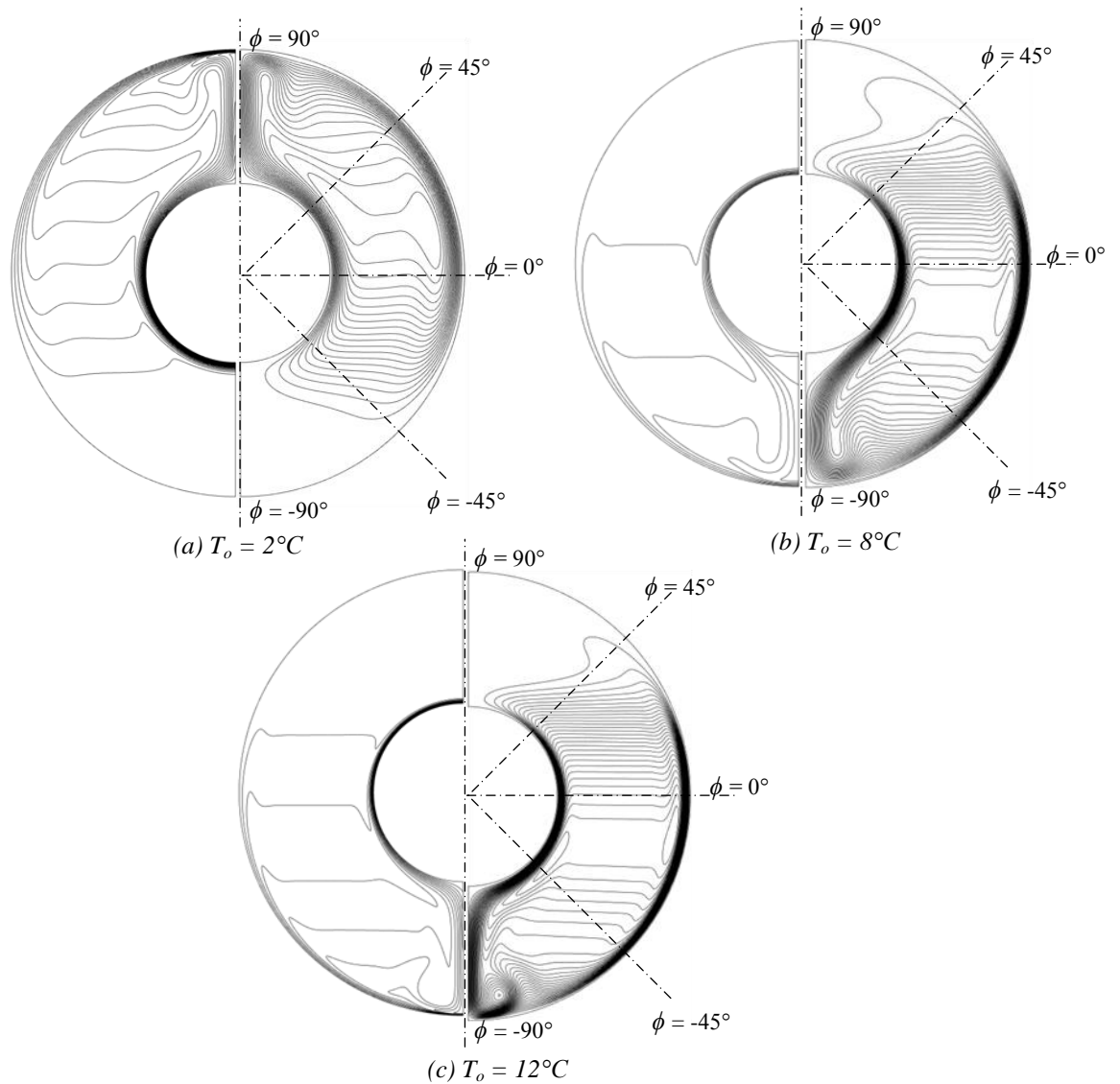
Figure 5.13 Temperature and velocity distribution for $L/r_i = 1.50$

$\phi = 90°$ $\phi = 45°$ $\phi = 0°$ $\phi = -90°$ $\phi = -45°$

(a) $T_o = 2°C$

$\phi = 90°$ $\phi = 45°$ $\phi = 0°$ $\phi = -90°$ $\phi = -45°$

(b) $T_o = 8°C$

$\phi = 90°$ $\phi = 45°$ $\phi = 0°$ $\phi = -90°$ $\phi = -45°$

(c) $T_o = 12°C$
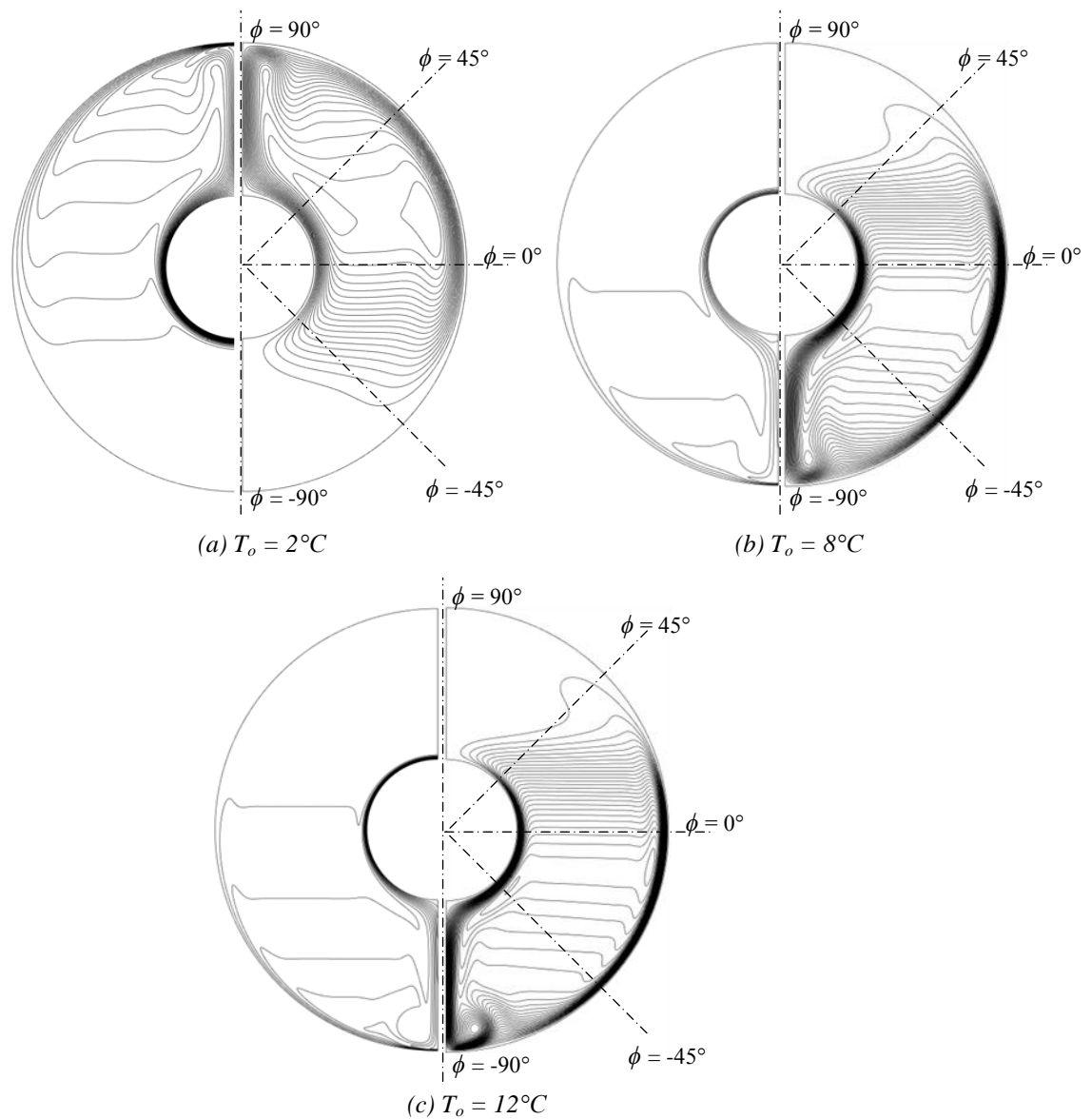
Figure 5.14 Temperature and velocity distribution for $L/r_i = 2.14$

In numerical analysis, temperature value of the inside sphere is determined constant and water phase change temperature 0°C. Water has biggest storage capacity per volume so it used as phase change material in cooling applications of the thermal energy storage. But mathematical simulations and engineering design is complicated because of the density of water has a peak value at 4°C. Notwithstanding the sphere annulus ratio, while surface temperature is higher than 4°C, two different flow circulation regions are occurred. This situation effects the

melting process time by increasing the effect of the heat transfer. In Figure 5.15, variation of the effective thermal conductivity is given in terms of temperature difference *(ΔT)* and the spacing ratio *(L/r_i)*.
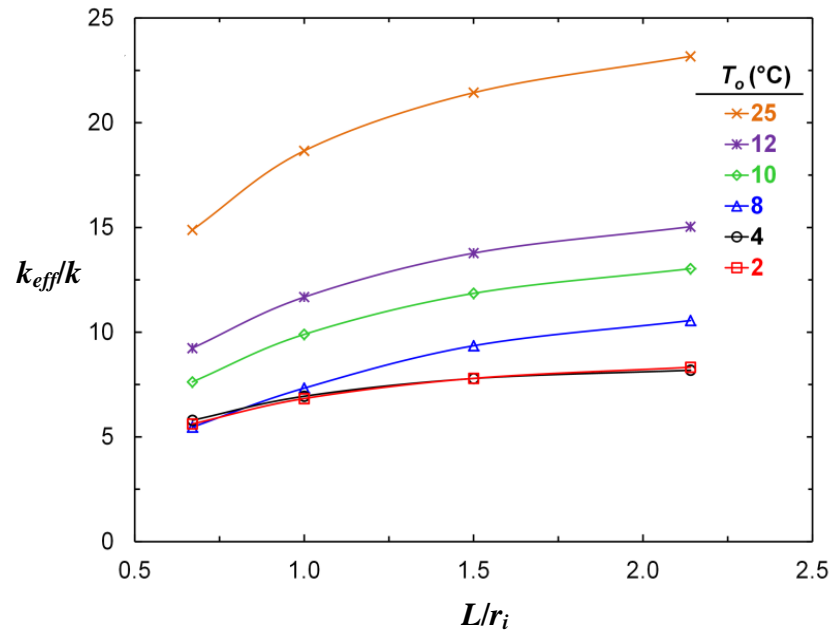
Figure 5.15 Effective thermal conductivity of water

It is clear that increasing the temperature difference and spacing ratio improve the impact of convective forces and enhances the k_{eff}. It is also interesting that for $T_o =$ 2°C and 4°C, the effective thermal conductivity values are almost identical for all spacing ratios. For the advancing temperature values, on the other hand, the effect of spacing ratio for a particular temperature value becomes clearer. For each outer surface temperature value, k_{eff} is obtained as a function of spacing ratio as 3rd order polynomial functions and the coefficients of these functions are given in Table 5.9.

Table 5.9 Effective thermal conductivity ($0.67 \leq L/r_i \leq 2.14$)

$k_{eff} = a\left(L/r_i\right)^3 + b\left(L/r_i\right)^2 + c\left(L/r_i\right) + d$				
T_o(°C)	*a*	*b*	*C*	*d*
2	0.77	-4.52	9.60	0.99
4	0.81	-4.7	9.61	1.22
8	0.0045	-1.94	8.85	0.40
10	1.18	-7.31	16.56	-0.56
12	1.27	-7.86	17.82	0.45
25	3.14	-17.05	33.28	-0.70

5.7 Numerical and Experimental Comparisons of the Effective Thermal Conductivity
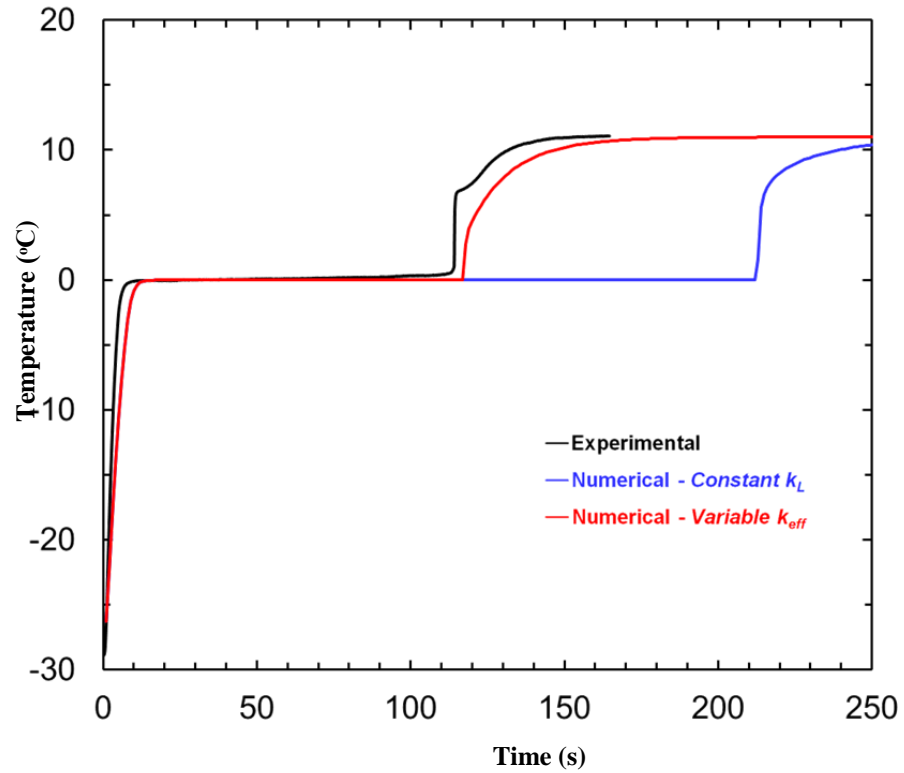
Figure 5.16 Comparison of the effective thermal conductivity with experimental results

As a last step, in order to test the validity of the equations that are suggested in Table 5.9, comparative results are given in Figure 5.16. Here, time-wise variation of the centre temperature of the sphere during the melting process is given together with the numerical results. In the numerical code, two different cases are considered. In the first one, the thermal conductivity of the water is kept constant during the whole process. It is clear that, for the constant k_l case, the resultant temperature variation is far from being capture the experimental one. On the other hand, with the implementation of effective thermal conductivity of water as a function of interface position in to the numerical code, the variation of temperature remarkably approaches to the experimental measurements.

CHAPTER SIX
CONCLUSIONS

In conclusion, two different numerical methods of one-dimensional phase change problems are examined during solidification process. Process are modelled one of the surface are considered as constant temperature one dimensional semi-infinite environment.

While we examined the obtained results, both of the numerical results are more close to the analytical solution with the increment of the grid number. Phase change problems show nonlinear feature so iterative solutions are needed to get better result in numerical solution. Comparing the numerical methods, temperature transformation method (TTM) gives better results according to solution time and accuracy of the results. Also higher percent errors obtained with analytical solutions are formed nearby of the phase change interface locations. The reason of the percent error nearby the interface location is arising latent heat effect during phase change process. Parametric study of this study is certified variation of Stefan number and Bi number. Both of the Stefan number and Bi number increment, interface movement of the phase change problem is accelerating.

In second study proposed the usage of effective thermal conductivity of water for inward process of water inside spherical container. Effective thermal conductivity values are evaluated in terms of the annulus ratio and the temperature differences. The comparative results reveal that the method yields reasonable results regarding the experimental measurements. The evaluated effective thermal conductivity combined with numerical code of the phase change problems in spherical coordinates and compared with experimental inward melting problem. Correlation of effective thermal conductivity gives reasonable results with experimental data.

REFERENCES

American Society of Heating, Refrigerating and Air-Conditioning Engineers (2001). *Ashrae Handbook Fundamentals*. Atlanta: Ashrae.

Assis, E., Katsman, L., Ziskind, G., & Letan, R., (2007). Numerical and experimental study of melting in a spherical shell. *International Journal of Heat and Mass Transfer*, *50*, 1790–1804.

Bilir, L., & Ilken, Z. (2005). Total solidification time of a liquid phase change material enclosed in cylindrical/spherical containers. *Applied Thermal Engineering, 25,* 1488-1502.

Bishop, E. H., Mack, L. R., & Scanlan, J.A. (1966). Heat transfer by natural convection between concentric spheres. *International Journal of Heat and Mass Transfer*, *9*, 649-662.

Cao, Y., & Faghri, A. (1990). Numerical analysis of phase change problems including natural convection. *Journal of Heat Transfer*, *112*, 812-816.

Cao, Y., & Faghri, A. A. (1991). A pcm/forced convection conjugate transient analysis of energy storage systems with annular and counter current flows. *Journal of Heat Transfer*, *113*, 37-42.

Carslaw, H. S., & Jaeger, J. C. (1959). *Conduction of heat in solids* (2nd ed.). London: Clarendon Press.

Incropera, F. P., Dewitt, D. P., Bergman, T. L., & Lavine, A. S. (2007). *Fundamentals of Heat and Mass Transfer* (6th ed.). USA: John Wiley & Sons, Inc.

Ismail, K. A. R., Henríquez, J. R., & Silva, T. M. (2003). A parametric study on ice formation inside a spherical capsule. *International Journal of Thermal Sciences*, *42*, 881-887.

Jiji, L. M., Rathjen, K. A. & Drzewiecki, T. (1970). Two-dimensional solidification in a corner. *International Journal of Heat and Mass Transfer, 13* (1) 215-218.

Özışık, M. N. (1993). *Heat conduction* (2nd ed.). New Jersey: John Wiley & Sons Inc.

Poots, G. (1962). An approximate treatment of a heat conduction problem involving a two-dimensional solidification front. *International Journal of Heat and Mass Transfer*, *5* (6), 525-531.

Seybert, C. D., & Evans, J. W. (2005). PIV measurements of velocity of water in the presence of ice and comparison with calculated values. *International Journal of Heat and Mass Transfer*, *48*, 67−73.

Voller, V. R., Cross, M., & Markatos, N. C. (1987). An enthalpy method for convection/diffusion phase change. *International Journal for Numerical Methods in Engineering*, *24*, 271-284.

Voller, V. R. & Prakash, C. (1987). A fixed grid numerical modelling methodology for convection diffusion mushy region phase change problems. *Heat and Mass Transfer*, *30* (8), 1709-1719.

Voller, V. R. & Swaminathan, C. R. (1991). General source-based method for solidification phase change. *Numerical Heat Transfer*, *19,* 175-189.

APPENDICES

A. Nomenclature

c	Specific heat [kJ/kgK]
C	Dimensionless heat capacity ($=(\rho c)/(\rho c)_L$)
g	Gravitational acceleration [m/s^2]
Gr	Grashof number ($=g\beta L^3(T_o-T_i)/\vartheta^2$)
h	Enthalpy [kJ/kg]
H	Total enthalpy [kJ/kg]
k	Thermal conductivity [W/mK]
K	Dimensionless thermal conductivity ($=k/k_L$)
L	Gap of annulus [m]
Nu	Nusselt number
q	Rate of heat transfer [W]
p	Pressure [Pa]
r	Radial axis direction [m]
R	Dimensionless radial axis ($=r/r_o$)
S	Dimensionless source term ($=(\rho c)/\left[(\rho c)_L(T_{in}-T_m)\right]$)
S'	Shape factor
Ste	Stefan number ($=c_L(T_{in}-T_m)/\Delta H$)
T	Temperature [°C]
t	Time [s]
u	Velocity [m/s]
x	Cartesian axis direction [m]

Special characters

ε	Convergence criteria
θ	Dimensionless temperature ($=(T-T_m)/(T_{in}-T_m)$)

$\delta\theta_m$	Dimensionless temperature range
δT_m	Temperature range
ΔH	Latent heat of fusion [kJ/kg]
ΔT	Temperature differences [K,^{o}C,^{o}F]
ρ	Density [kg/m^3]
θ	Dimensionless temperature
ϕ	Angular position [^{o}]
μ	Dynamic viscosity [kg/ms]
ϑ	Kinematic viscosity [m^2/s]
τ	Dimensionless time $\left(=\left(k/c\rho\right)_{L}t/r_{o}\right)$

Subscripts or
Superscripts

eff	Effective
o	Previous time step value
*	Dimensional form
e	East node
w	West node
i	Inner
in	Initial condition
l	Liquid phase
m	Melting or Mushy region
n	Description of coordinate type
o	Outer
s	Solid phase

B. Matlab Code

```matlab
%% IMPORT Numerical Results of Reference Work %%
close all

%% Type of the Geometry
% N_geo = 0 Cartesian / N_geo = 1 Cylindrical / N_geo = 2 Spherical
N_geo = 2;
%% Thermal Boundary Conditions
Tm = 273.15; Tin = 298.15; Tinf = 263.15; dTm = 0.01;
h_conv = 218.7;
%% Thermo-physical Properties
kl = 0.567; ks = 1.88; cl = 4210; cs = 2040; ro_s = 916.8; ro_l = 999.8;
dH = 333500;
alfa_l = kl/ro_l/cl;
%% Geometric Dimensions
radius = 0.03; grow_rate = 0.95; n = 200;
%% Time step & Maximum number of iterations
t = 10000;  dt = 1; n_time = t/dt; max_iter = 10000;
%% Non-Dimensional Parameters
Csl = (ro_s*cs)/(ro_l*cl); Ksl = ks/kl;
Ste = cl*(Tin - Tm)/dH;
dTeta = dTm/(Tin - Tm);

Teta_inf = (Tinf - Tm)/(Tin - Tm); Teta_in = (Tin - Tm)/(Tin - Tm);
Teta_m = (Tm - Tm)/(Tin - Tm);

to = alfa_l*t/(radius^2); d_to = alfa_l*dt/(radius^2);
Biot = h_conv*radius/kl;
%% Definition of the Matrices
% Gometric
Rp = zeros(1,n); Rn = zeros(1,n); Rs = zeros(1,n);
DRn = zeros(1,n); DRs = zeros(1,n);

% TDMA
a = zeros(1,n); b = zeros(1,n); c = zeros(1,n); d = zeros(1,n);

% Thermal
C = zeros(1,n); C0 = zeros(1,n);
K = zeros(1,n); K0 = zeros(1,n);
Kn = zeros(1,n); Ks = zeros(1,n);
S = zeros(1,n); S0 = zeros(1,n);
H = zeros(1,n); H0 = zeros(1,n);
Teta = ones(1,n)*Teta_in; Teta0 = ones(1,n)*Teta_in;
Teta_iter = zeros(1,n);

for i=1:n
    Teta_iter(i) = 0.0; C(i) = 0.0; K(i) = 0.0; H(i) = 0.0; S(i) = 0.0;
    C0(i) = 0.0; K0(i) = 0.0; H0(i) = 0.0; S0(i) = 0.0;
    Kn(i) = 0.0; Ks(i) = 0.0;
    Rp(i) = 0.0; Rn(i) = 0.0; Rs(i) = 0.0; DRn(i) = 0.0; DRs(i) = 0.0;
end
%% Generate Non-Uniform Structured Mesh
[Rp, Rn, Rs, DRn, DRs] = mesh(grow_rate, n);
%% Define Windows
figHandle1 = figure;
```

```matlab
set(figHandle1,'Name','Variation of Temperature','NumberTitle','off')
% figHandle2 = figure;
% set(figHandle2,'Name','Time-wise Variation of Temperature','NumberTitle','off')
% figHandle3 = figure;
% set(figHandle3,'Name','Variation of Error','NumberTitle','off')
%% Draw the results of the reference work on Fig2.
figure(figHandle1);
xlabel('Time (s)');
ylabel('Surface Temperature (Celcius)');
y = Tinf:(Tin - Tinf)/5:Tin;
%plot(bilir_x, bilir_y);
%hold on
%% SOLUTION ALGORITHM
for k=1:n_time
    for j=1:max_iter
    % Evaluate Faghri Parameters
    [C, C0, S, S0, K, K0, H, H0] = Faghri(Teta, Teta0, Ksl, Csl, Ste, dTeta, n);

    % Harmonik Mean
    [Kn, Ks] = harmonik(Rp, Rs, Rn, K, n, N_geo);

    % Coefficients of Matrix
    [an, as, ap, b] = coefficients(C, C0, Kn, Ks, Rp, Rn, Rs, DRn, DRs, Teta0, S, S0, Biot, Teta_inf,
d_to, n, N_geo);

    % TDMA
    [Teta_iter] = tdma(-as, ap, -an, b, n);

    % Check the Convergence
    NC=0;

    UR = 0.1;
    if j > 50
       UR = 0.05;
    elseif j > 200
       UR = 0.02;
    elseif j > 300
       UR = 0.01;
    elseif j > 500
       UR = 0.005;
    elseif j > 1000
       UR = 0.002;
    elseif j > 3000
       UR = 0.001;
    elseif j > 4000
       UR = 0.0005;
    elseif j > 5000
       UR = 0.0001;
    elseif j > 8000
       UR = 0.00001;
    end

    MaxHata = 0.0; Hata = 0.0;
    for i=1:n
       Hata = abs(abs(Teta(i)) - abs(Teta_iter(i)))/abs(Teta_iter(i))*100;
       if  abs(Hata) > 10^-8
          NC = NC + 1;
          Teta(i) = UR*Teta_iter(i) + (1 - UR)*Teta(i);
```

```matlab
            if Hata > MaxHata
                MaxHata = Hata;
            end
        end
    end

    if NC == 0
        break
    end
 end


    [err]=ebalance(H, H0, Rn, Rs, Biot, Teta, Teta_inf, d_to, n);

Teta0 = Teta;

if round(k/5)*5 == k
   [T_boyutlu] = plot_graph(Teta, c_time, Tin, Tm, Tinf, n, figHandle1, err);
end
%% Print on Command Window
c_time = d_to*k*radius^2/alfa_l;
c_time

%% Print on a File
filename = fullfile('sphere.txt');
fid =  fopen (filename, 'a');

fprintf(fid,'%f %f %f %f \r\n',c_time, Teta(1)*(Tin - Tm) + Tm, Teta(n)*(Tin - Tm) + Tm, err);
fclose(fid);

end
```